Composite Structures 280 (2022) 114925

Contents lists available at ScienceDirect

Composite Structures

journal homepage: www.elsevier.com/locate/compstruct

Vibration analysis of auxetic laminated plate with magneto-electro-elastic face sheets subjected to blast loading

Ngo Dinh Dat [a], Tran Quoc Quan [a,b,*], Nguyen Dinh Duc [c]

[a] Phenikaa Institute for Advanced Study (PIAS), Phenikaa University, Hanoi 12116, Viet Nam
[b] Faculty of Mechanical Engineering and Mechatronics, Phenikaa University, Hanoi 12116, Viet Nam
[c] Department of Engineering and Technology in Constructions and Transportation –VNU Hanoi, University of Engineering and Technology, 144 – Xuan Thuy, Cau Giay, Hanoi, Viet Nam

ARTICLE INFO

Keywords:
Nonlinear vibration analysis
Auxetic laminated plate
Magneto-electro-elastic face sheets
Negative Poisson's ratio
Blast loading

ABSTRACT

Mathematic modeling and analytical approach are presented for nonlinear vibration analysis of laminated plate with auxetic honeycomb core and magneto-electro-elastic face sheets supported by Pasternak-type elastic foundations. The laminated plate is subjected to the simultaneous action of blast, thermal, electric and magnetic loadings. The mechanical properties of auxetic core including negative Poisson's ratio are assumed to depend on the geometrical parameters of the unit cells and elastic modulus of original material. The volume fraction of two components of each magneto-electro-elastic face sheet is chosen equally. The nonlinear motion equations and the geometrical compatibility equation are established by using Reddy's higher order shear deformation plate theory taking into account the coupling between elastic, electric and magnetic fields. The analytical vibration solutions for the auxetic laminated plate can be obtained by using Galerkin and fourth-order Runge – Kutta methods. The numerical results are conducted to investigate the effect of geometrical and material parameters, elastic foundations, temperature increment, magnetic and electric potentials on the vibration characteristics of the auxetic laminated plate.

1. Introduction

Due to the rapid increase of terrorist activities and threats in recent decades, the civilian buildings and military constructions have seriously affected by explosions from bombs and chemical gases. As a result, the problems of blast phenomenon, mechanisms of blast loading and design important structures to resist blast loading have attracted great interest of scientific and military community all over the world. Gholipour et al. [1] assessed the vulnerability of a reinforced concrete girder bridge pier using high- and moderate- resolution finite element simulations in LS-DYNA under the combination of vessel collisions and blast loadings. It was found that the pier undergoes more severe localized failure when both impact and blast loads were applied at the same elevation on the pier column which is more likely to occur during barge collisions. Maazoun et al. [2] presented a new experimental setup developed in order to study blast driven bond interaction between carbon fiber reinforced polymer and concrete. Further, Roy and Matsagar [3] proposed a probabilistic framework which utilizes the effects of uncertainties in the system to compute the failure probabilities of a reinforced concrete structural member under extreme blast loading. Lam et al. [4] developed the modelling of blast pressure for engineering applications. An important contribution from this study was the identification of the direct relationship between the corner period and the clearing time for the blast. Based on finite element method and smoothed particle hydrodynamics, Karmakar and Shaw [5] investigated the response of reinforced concrete plates subjected to blast loading through a hybrid discretization. Recently, Gao et al. [6] developed a numerical model by using the hydrocode AUTODYN to investigate the influences of aspect ratio and orientation on the free air blast loads generated from center-initiated cylindrical charges. Le et al. [7] mimicked numerous features from the cross-lamellar structure of conch to enhance the performance of cross-laminated timber under blast loading; Xiao et al. [8] investigated the blast loads on a two-storeyed reinforced concrete and masonry building with a gable roof through five full-scale experiments and numerical.

Auxetic materials with the unique shape of atomic structure have

* Corresponding author at: Phenikaa Institute for Advanced Study (PIAS), Phenikaa University, Hanoi 12116, Viet Nam and Faculty of Mechanical Engineering and Mechatronics, Phenikaa University, Hanoi 12116, Viet Nam.

E-mail address: quan.tranquoc@phenikaa-uni.edu.vn (T. Quoc Quan).

https://doi.org/10.1016/j.compstruct.2021.114925
Received 10 September 2021; Received in revised form 19 October 2021; Accepted 28 October 2021
Available online 6 November 2021

preeminent features such as negative Poisson's ratio and ability to absorb the shock waves. Auxetic materials become the ideal choices for essential components of structures subjected to the potential extreme loading conditions including blast loading. Recently, large number of studies has been conducted on the mechanical properties and behaviors of auxetic structures. Usta et al. [9] described the low-velocity impact behavior of composite sandwich panels with different types of auxetic and non-auxetic prismatic core structures in which sandwich panels had been manufactured with carbon/fiber epoxy composite face sheets, polyurethane rigid foam core or 3D printed PLA plastic cellular honeycombs head. Dong et al. [10] proposed a novel strategy to fabricate continuous fiber-reinforced electro-induced shape memory auxetic composites by combining conductive filaments and continuous carbon fiber through 3D printing technology. Based on finite element approach, Dutta et al. [11] discussed about the single cell honeycomb and re-entrant configurations and used analytical formulations to calculate the Poisson's ratio for various structures. Li et al. [12,13] presented full-scale modeling and and nonlinear finite element analysis to investigate the nonlinear dynamic response and large amplitude vibration of sandwich plates with auxetic 3D lattice core. Besides, Gao et al. [14] developed an effective and efficient computational design framework for auxetic composites with the tri-material using isogeometric topology optimization method, in which a tri-material topology representation model is constructed by non-uniform rationally B-splines to effectively represent micro-structural topology with clear and smooth boundaries. Quyen et al. [15] studied the nonlinear free and forced vibration of sandwich cylindrical panel on visco-Pasternak foundations in thermal environment subjected to blast load; Li et al. [16] presented multi-scale modeling and nonlinear low-velocity impact analysis of sandwich plates with graphene reinforced composite face sheets and functionally graded auxetic 3D lattice cores. Yang et al. [17] reported a study on the large amplitude nonlinear vibration of carbon nanotube-reinforced composite laminated plates with negative Poisson's ratios in thermal environments based on the Reddy's third order shear deformation theory. An analytical approach is proposed to investigate the nonlinear dynamic analysis of porous eccentrically stiffened double curved shallow auxetic shells with negative Poisson's ratio subjected to blast, mechanical and thermal loads resting on visco-Pasternak foundation model in the work of Cong and Duc [18]. Based on Mindlin plate theory and finite element method, Tran et al. [19] investigated dynamic response analysis of sandwich composite plates with auxetic honeycomb core resting on the elastic foundation under moving oscillator load. Yu and Shen [20] introduced a study on the large amplitude vibration and nonlinear bending behaviors of hybrid laminated plates made of carbon nanotube-reinforced composite layers bonded with metal layer on the top surface. Further, Gohar et al. [21] presented experimental and finite element analyses on performance of 3D printed topologically optimized novel auxetic structures under compressive loading. In 2021, Gao and Liao [22] proposed a thin walled structure filled with double arrowed auxetic structure and investigated the energy absorption characteristics.

With the development of science and technology, smart materials which express the ability to respond to an external stimulus are found to meet modern technical requirements. Magneto-electro-elastic material which consists of piezoelectric and piezomagnetic phases is one potential class of smart materials. The applications of magneto-electro-elastic material are increasing continuously in various fields such as sensors, automobiles, energy harvesting, medical devices and civil structures. Zur et al. [23] studied the free vibration and buckling responses of functionally graded nanoplates with magneto-electro-elastic coupling using a nonlocal modified sinusoidal shear deformation plate theory including the thickness stretching effect. Based on nonlocal elasticity theory, Arefi and Amabili [24] investigated the three-dimensional magneto-electro-elastic bending and buckling analyses of three-layered doubly curved nanoshells. Vinyas et al. [25] researched the influence of piezoelectric interphase thickness on the coupled frequency response of three-phase smart magneto-electro-elastic plates with the aid of Reddy's third-order shear deformation theory. Besides, Zhu et al. [26] dealt with the post-buckling analysis of magneto-electro-elastic composite cylindrical shells subjected to multi-field coupled loadings using the higher order shear deformation theory; Dat et al. [27] presented an analytical approach on the nonlinear magneto-electro-elastic vibration of smart sandwich plate which consisted of a carbon nanotube reinforced nanocomposite core integrated with two magneto-electro-elastic face sheets. Recently, Zhou et al. [28] used the cell-based smoothed finite element method and the asymptotic homogenization method to accurately simulate the responses of 1–3 type magneto-electro-elastic structure under dynamic load. Ye et al. [29] investigated the bending response performances of the magneto-electro-elastic laminated plates resting on the Winkler foundation or the elastic half-space subjected to a transverse mechanical loading. Shojaeefard et al. [30] predicted the first natural frequency and the critical angular velocity of a thermo-electro-magneto-elastic single-layer cylindrical nano-shell resting on a Winkler foundation based on the Hamiltonian principle and by using first shear deformation theories in conjunction with modified couple stress theory. Chen et al. [31] proposed the state-vector approach to analyze the free vibration of magneto-electro-elastic laminate plates. Xu and Meng [32] proposed a size-dependent elastic theory for magneto-electro-elastic nano-materials.

The model of laminated plate with auxetic honeycomb core and magneto-electro-elastic face sheets is introduced in this paper for the first time. The laminated auxetic plate is subjected to the combination of blast, thermal, electric and magnetic loadings. The governing equations of nonlinear vibration problem are derived based on the Reddy's higher order shear deformation plate theory. The analytical solutions are proposed and the expressions of vibration characteristics such as natural frequency, relationship between frequency ratio and dimensionless amplitude, and dynamic response are obtained by using Galerkin and Runge - Kutta methods. The numerical results are conducted to investigate the effect of geometrical and material parameters, elastic foundations and external loadings on the vibration of laminated auxetic plate.

2. Theoretical formulations

A laminated plate with length of a, width of b and total thickness of h has been considered in Fig. 1. The laminated plate consists of an auxetic core and two magneto-electro-elastic face sheets. Each face sheet has N plies in which all plies have the same thickness. The thickness of auxetic core layer and each face sheet are denoted by h_c and h_f, respectively. A Cartesian coordinate system (x, y, z) is established in which x, y and z are in the length, width and thickness directions, respectively, and (x, y) plane is located on the mid-surface of the laminated plate.

The auxetic core layer is made up of honeycomb unit cells. The model of single unit cell is shown in Fig. 2 where t, d, l and θ are denoted for the thickness of the relative cell wall, the length of the vertical cell rib, the length of the inclined cell rib and the inclined angle, respectively.

The mechanical properties of the honeycomb auxetic core layer such as Young's modulus, shear modulus, negative Poisson's ratio and thermal expansion coefficients are assumed to depend on the geometrical parameters of the single unit cell as [15,19]

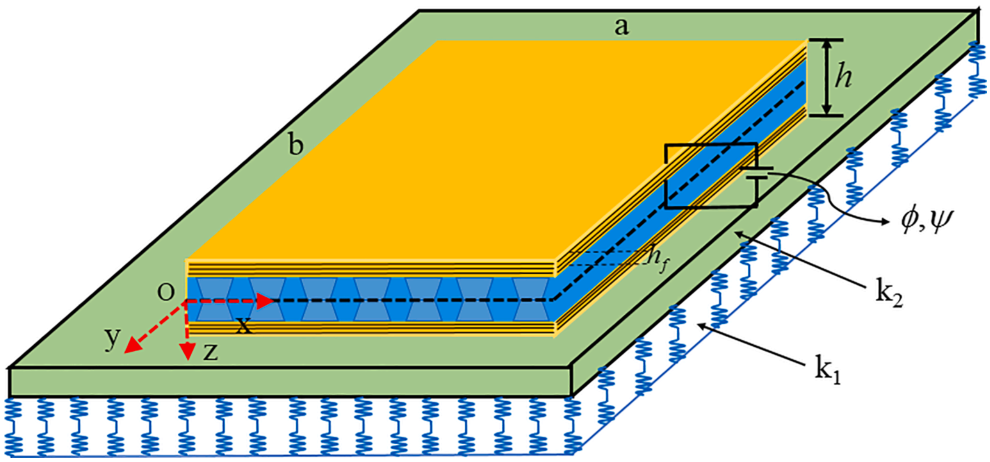

Fig. 1. Geometry and coordinate system of the auxetic laminated plate with magneto-electro-elastic face sheets.

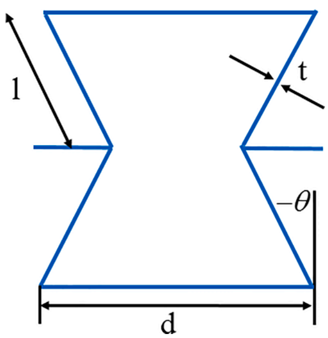

Fig. 2. Model of auxetic single unit cell.

$$E_1^a = E\frac{\left(\frac{t}{l}\right)^3\left(\frac{d}{l}-sin\theta\right)}{cos^3\theta\left[1+\left(tan^2\theta+\frac{d}{l}sec^2\theta\right)\eta_3^2\right]}, E_2^a = E\frac{\left(\frac{t}{l}\right)^3}{cos\theta\left(\frac{d}{l}-sin\theta\right)\left(tan^2\theta+\left(\frac{t}{l}\right)^2\right)},$$

$$G_{12}^a = E\frac{\left(\frac{t}{l}\right)^3}{\frac{d}{l}\left(1+2\frac{d}{l}\right)cos\theta}; v_{12}^a = -\frac{sin\theta\left(1-\left(\frac{t}{l}\right)^2\right)\left(\frac{d}{l}-sin\theta\right)}{cos^2\theta\left[1+\left(tan^2\theta+sec^2\theta\frac{d}{l}\right)\left(\frac{t}{l}\right)^2\right]},$$

$$G_{23}^a = G\frac{\left(\frac{t}{l}\right)cos\theta}{\frac{d}{l}-sin\theta}, G_{13}^a = G\frac{\left(\frac{t}{l}\right)}{2cos\theta}\left[\frac{\frac{d}{l}-sin\theta}{1+2\frac{d}{l}}+\frac{\frac{d}{l}+2sin^2\theta}{2\left(\frac{d}{l}-sin\theta\right)}\right],$$

$$v_{21}^a = -\frac{sin\theta\left(1-\left(\frac{t}{l}\right)^2\right)}{\left(tan^2\theta+\left(\frac{t}{l}\right)^2\right)\left(\frac{d}{l}-sin\theta\right)}, \rho^a = \rho\frac{\left(\frac{t}{l}\right)\left(\frac{d}{l}+2\right)}{2cos\theta\left(\frac{d}{l}-sin\theta\right)},$$

$$\alpha_1^a = \alpha\frac{\frac{t}{l}\cos\theta}{sin\theta+\frac{d}{l}}, \alpha_2^a = \alpha\frac{\frac{t}{l}\left(\frac{d}{l}+sin\theta\right)}{\left(2\frac{d}{l}+1\right)\cos\theta}, \tag{1}$$

in which the notation " a " refers to auxetic honeycomb core layer; E, G and ρ are Young's modulus, shear modulus and mass density of the original material of auxetic core layer.

The magneto-electro-elastic face sheet is a combination of Barium Titanate ($BaTiO_3$) with piezoelectric property and Cobalt Ferric oxide ($CoFe_2O_4$) with piezomagnetic property. The material properties of the magneto-electro-elastic face sheet which depend on the volume fraction of two components are expressed in Table 1 [25,27].

Table 1
Mechanical properties of magneto-electro-elastic face sheet.

Material properties	Notation	Values
Elastic constants (GPa)	$C_{11}^f = C_{22}^f$	220
	$C_{12}^f = C_{13}^f = C_{23}^f$	120
	C_{33}^f	215
	$C_{44}^f = C_{55}^f$	45
	C_{66}^f	0
Piezoelectric constants (C/m^2)	e_{31}^f	-3.5
	e_{33}^f	9.0
	e_{15}^f	0
Dielectric constants (C/Nm^2)	$\eta_{11}^f = \eta_{22}^f$	0.85×10^{-9}
	η_{33}^f	6.3×10^{-9}
Magnetic permeability (Ns^2/C^2)	$\mu_{11}^f = \mu_{22}^f$	-2×10^{-4}
	μ_{33}^f	0.9×10^{-4}
Piezomagnetic constants (N/Am)	q_{31}^f	350
	q_{33}^f	320
	q_{15}^f	200
Magneto-electric constants (Ns/VC)	$m_{11}^f = m_{22}^f$	5.5×10^{-12}
	m_{33}^f	2600×10^{-12}
Pyroelectric constant (C/m^2K)	p_3^f	7.8×10^{-7}
Pyromagnetic constant (C/m^2K)	λ_3^f	-23×10^{-5}
Thermal expansion coefficients (K^{-1})	$\alpha_1^f = \alpha_2^f$	12.3×10^{-6}
	α_3^f	8.2×10^{-6}
Density (kg/m^3)	ρ_f	5500

3. Basic equations

3.1. Displacement field

Based on the Reddy's higher order shear deformation plate theory, the consistent Donnell nonlinear strain components across the plate thickness at a distance z from the mid-plane are [37,38]

$$\begin{bmatrix}\varepsilon_x\\ \varepsilon_y\\ \gamma_{xy}\end{bmatrix} = \begin{bmatrix}\varepsilon_x^0\\ \varepsilon_y^0\\ \gamma_{xy}^0\end{bmatrix} + z\begin{bmatrix}k_x^1\\ k_y^1\\ k_{xy}^1\end{bmatrix} + z^3\begin{bmatrix}k_x^3\\ k_y^3\\ k_{xy}^3\end{bmatrix}, \begin{bmatrix}\gamma_{xz}\\ \gamma_{yz}\end{bmatrix} = \begin{bmatrix}\gamma_{xz}^0\\ \gamma_{yz}^0\end{bmatrix} + z^2\begin{bmatrix}k_{xz}^2\\ k_{yz}^2\end{bmatrix}, \tag{2}$$

where

$$\begin{bmatrix} \varepsilon_x^0 \\ \varepsilon_y^0 \\ \gamma_{xy}^0 \end{bmatrix} = \begin{bmatrix} \dfrac{\partial u}{\partial x} + \dfrac{1}{2}\left(\dfrac{\partial w}{\partial x}\right)^2 \\ \dfrac{\partial v}{\partial y} + \dfrac{1}{2}\left(\dfrac{\partial w}{\partial y}\right)^2 \\ \dfrac{\partial u}{\partial y} + \dfrac{\partial v}{\partial x} + \dfrac{\partial w}{\partial x}\dfrac{\partial w}{\partial y} \end{bmatrix}, \quad \begin{bmatrix} \gamma_{xz}^0 \\ \gamma_{yz}^0 \end{bmatrix} = \begin{bmatrix} \dfrac{\partial w}{\partial x} + \phi_x \\ \dfrac{\partial w}{\partial y} + \phi_y \end{bmatrix},$$
$$\begin{bmatrix} k_x^1 \\ k_y^1 \\ k_{xy}^1 \end{bmatrix} = \begin{bmatrix} \dfrac{\partial \phi_x}{\partial x} \\ \dfrac{\partial \phi_y}{\partial y} \\ \dfrac{\partial \phi_x}{\partial y} + \dfrac{\partial \phi_y}{\partial y} \end{bmatrix}, \quad \begin{bmatrix} k_x^3 \\ k_y^3 \\ k_{xy}^3 \end{bmatrix} = -c_1 \begin{bmatrix} \dfrac{\partial \phi_x}{\partial x} + \dfrac{\partial^2 w}{\partial x^2} \\ \dfrac{\partial \phi_y}{\partial y} + \dfrac{\partial^2 w}{\partial y^2} \\ \dfrac{\partial \phi_x}{\partial y} + \dfrac{\partial \phi_y}{\partial y} + 2\dfrac{\partial^2 w}{\partial x \partial y} \end{bmatrix}, \quad \begin{bmatrix} k_{xz}^2 \\ k_{yz}^2 \end{bmatrix} = -3c_1 \begin{bmatrix} \dfrac{\partial w}{\partial x} + \phi_x \\ \dfrac{\partial w}{\partial y} + \phi_y \end{bmatrix}, \tag{3}$$

with $c_1 = 4/(3h^2)$; u, v and w are the mid-plane displacements in the x, y and z directions, respectively; the rotations of the transverse normal to the middle surface with respect to the y and $x-$ axes are denoted by ϕ_x and ϕ_y , respectively.

3.2. Constitutive equations

The auxetic core layer is assumed to be hard material. The stress--strain relations of the auxetic core layer taking into account the effect of temperature can be expressed as

$$\begin{bmatrix} \sigma_{xx} \\ \sigma_{yy} \\ \sigma_{xy} \\ \sigma_{xz} \\ \sigma_{yz} \end{bmatrix}_c = \begin{bmatrix} Q_{11}^c & Q_{12}^c & 0 & 0 & 0 \\ Q_{12}^c & Q_{22}^c & 0 & 0 & 0 \\ 0 & 0 & Q_{66}^c & 0 & 0 \\ 0 & 0 & 0 & Q_{44}^c & 0 \\ 0 & 0 & 0 & 0 & Q_{55}^c \end{bmatrix} \left[\begin{bmatrix} \varepsilon_{xx} \\ \varepsilon_{yy} \\ \varepsilon_{xy} \\ \varepsilon_{xz} \\ \varepsilon_{yz} \end{bmatrix}_c - \begin{bmatrix} \alpha_{11}^c \Delta T \\ \alpha_{22}^c \Delta T \\ 0 \\ 0 \\ 0 \end{bmatrix} \right], \tag{4}$$

in which

$$Q_{11}^c = \frac{E_{11}^a}{1-\nu_{12}^a \nu_{21}^a}, \ Q_{12}^c = \frac{\nu_{21}^a E_{11}^a}{1-\nu_{12}^a \nu_{21}^a}, \ Q_{22}^c = \frac{E_{22}^a}{1-\nu_{12}^a \nu_{21}^a}, \ Q_{44}^c = G_{23}^a,$$
$$Q_{55}^c = G_{13}^a, \ Q_{66}^c = G_{12}^a. \tag{5}$$

For magneto-electro-elastic face sheets, the constitutive equations which show the relationship between stress components, electric displacement and the magnetic flux and strain components, elastic, electric and magnetic fields are expressed in the following forms [25,27]

$$\begin{aligned} \sigma_{xx}^f &= \overline{C_{11}}\varepsilon_{xx}^f + \overline{C_{12}}\varepsilon_{yy}^f - \overline{e_{31}}E_z - \overline{q_{31}}H_z - \overline{\alpha_1}\Delta T, \\ \sigma_{yy}^f &= \overline{C_{11}}\varepsilon_{xx}^f + \overline{C_{22}}\varepsilon_{yy}^f - \overline{e_{32}}E_z - \overline{q_{32}}H_z - \overline{\alpha_2}\Delta T, \\ \tau_{xy}^f &= 2\sigma_{xy}^f = \overline{C_{66}}\gamma_{xy}^f, \\ \tau_{yz}^f &= \overline{C_{44}}\gamma_{yz}^f - \overline{e_{24}}E_y - \overline{q_{24}}H_y, \\ \tau_{xz}^f &= \overline{C_{55}}\gamma_{xz}^f - \overline{e_{15}}E_x - \overline{q_{15}}H_x, \\ D_x^f &= \overline{e_{15}}\gamma_{xz}^f + \overline{\eta_{11}}E_x + \overline{m_{11}}H_x + \overline{p_1}\Delta T, \\ D_y^f &= \overline{e_{24}}\gamma_{yz}^f + \overline{\eta_{22}}E_y + \overline{m_{22}}H_y + \overline{p_2}\Delta T, \\ D_z^f &= \overline{e_{31}}\varepsilon_{xx}^f + \overline{e_{32}}\varepsilon_{yy}^f + \overline{\eta_{33}}E_z + \overline{m_{33}}H_z + \overline{p_3}\Delta T, \\ B_x^f &= \overline{q_{15}}\gamma_{xz}^f + \overline{m_{11}}E_x + \overline{\mu_{11}}H_x + \overline{\lambda_1}\Delta T, \\ B_y^f &= \overline{q_{24}}\gamma_{yz}^f + \overline{m_{22}}E_y + \overline{\mu_{22}}H_y + \overline{\lambda_2}\Delta T, \\ B_z^f &= \overline{q_{31}}\varepsilon_{xx}^f + \overline{q_{32}}\varepsilon_{yy}^f + \overline{m_{33}}E_z + \overline{\mu_{33}}H_z + \overline{\lambda_3}\Delta T, \end{aligned} \tag{6}$$

in which notation "f" denotes for magneto-electro-elastic face sheets; the details of coefficients $\overline{C_{ij}}$ $(ij = 11, 12, 22, 44, 55, 66)$, $\overline{e_{kl}}(kl = 31, 32, 24, 15)$, $\overline{q_{kl}}(kl = 31, 32, 24, 15)$,$\overline{\alpha_i}(i = 1, 2)$, $\overline{\eta_{ij}}$, $\overline{m_{ij}}$, $\overline{\mu_{ij}}$ $(ij = 11, 22, 33)$, $\overline{p_i}$, $\overline{\lambda_i}$ and $\overline{\zeta_i}$ $(i = 1, 2, 3)$ may be found in Appendix A.

The electric and magnetic fields may be expressed from the electric and magnetic potentials as [25,27]

$$\{E_i, H_i\} = \left\{ -\widetilde{\Phi}_{,i}, -\widetilde{\Psi}_{,i} \right\}, i = x, y, z, \tag{7}$$

where the electric potential and magnetic potentials $\widetilde{\Phi}$ and $\widetilde{\Psi}$ are assumed to have the following forms

$$\begin{aligned} \widetilde{\Phi}(x,y,z,t) &= -cos(\beta z)\Phi(x,y,t) + \frac{2z\phi_0}{h}, \\ \widetilde{\Psi}(x,y,z,t) &= -cos(\beta z)\Psi(x,y,t) + \frac{2z\psi_0}{h}, \end{aligned} \tag{8}$$

in which $\beta = \frac{\pi}{h}$; $\Phi(x,t), \Psi(x,t)$ are the spatial variation of the electric and magnetic potentials, respectively. Besides, ϕ_0 and ψ_0 are the initial electric and magnetic potentials, respectively.

Substituting Eq. (8) into Eq. (7), the electric and magnetic fields can be obtained by following expression

$$\begin{aligned} \begin{Bmatrix} E_x \\ E_y \\ E_z \end{Bmatrix} &= \begin{Bmatrix} -\dfrac{\partial \widetilde{\Phi}}{\partial x} \\ -\dfrac{\partial \widetilde{\Phi}}{\partial y} \\ -\dfrac{\partial \widetilde{\Phi}}{\partial z} \end{Bmatrix} = \begin{Bmatrix} cos(\beta z)\dfrac{\partial \Phi}{\partial x} \\ cos(\beta z)\dfrac{\partial \Phi}{\partial y} \\ -\beta sin(\beta z)\Phi - \dfrac{2\phi_0}{h} \end{Bmatrix}, \\ \begin{Bmatrix} H_x \\ H_y \\ H_z \end{Bmatrix} &= \begin{Bmatrix} -\dfrac{\partial \widetilde{\Psi}}{\partial x} \\ -\dfrac{\partial \widetilde{\Psi}}{\partial y} \\ -\dfrac{\partial \widetilde{\Psi}}{\partial z} \end{Bmatrix} = \begin{Bmatrix} cos(\beta z)\dfrac{\partial \Psi}{\partial x} \\ cos(\beta z)\dfrac{\partial \Psi}{\partial y} \\ -\beta sin(\beta z)\Psi - \dfrac{2\psi_0}{h} \end{Bmatrix}, \end{aligned} \tag{9}$$

The force and moment resultants of the auxetic laminated plate are determined as follows [37,38]

$$(N_i,M_i,P_i)=\int_{-\frac{h_c}{2}-h_f}^{-\frac{h_c}{2}}\sigma_i^f\left(1,z,z^3\right)dz+\int_{-\frac{h_c}{2}}^{\frac{h_c}{2}}\sigma_i^C\left(1,z,z^3\right)dz$$
$$+\int_{\frac{h_c}{2}}^{\frac{h_c}{2}+h_f}\sigma_i^f\left(1,z,z^3\right)dz, i=xx,yy,xy,$$
$$(Q_i,R_i)=\int_{-\frac{h_c}{2}-h_f}^{-\frac{h_c}{2}}\sigma_{iz}^f\left(1,z^2\right)dz+\int_{-\frac{h_c}{2}}^{\frac{h_c}{2}}\sigma_{iz}^C\left(1,z^2\right)dz+\int_{\frac{h_c}{2}}^{\frac{h_c}{2}+h_f}\sigma_{iz}^f\left(1,z^2\right)dz, i=x,y, \tag{10}$$

Substituting Eq. (2) into Eqs. (4) and (6) then the results into Eq. (10), the internal forces and moments are given as

$$\begin{aligned}
N_x&=A_{11}\varepsilon_x^0+A_{12}\varepsilon_y^0+B_{11}k_x^1+B_{12}k_y^1+E_{11}k_x^3+E_{12}k_y^3-\Phi_1E_z-\Gamma_1H_z-\alpha_1\Delta T,\\
N_y&=A_{12}\varepsilon_x^0+A_{22}\varepsilon_y^0+B_{12}k_x^1+B_{22}k_y^1+E_{12}k_x^3+E_{22}k_y^3-\Phi_2E_z-\Gamma_2H_z-\alpha_2\Delta T,\\
N_{xy}&=A_{66}\gamma_{xy}^0+B_{66}k_{xy}^1+E_{66}k_{xy}^3,\\
M_x&=B_{11}\varepsilon_x^0+B_{12}\varepsilon_y^0+D_{11}k_x^1+D_{12}k_y^1+F_{11}k_x^3+F_{12}k_y^3-\Phi_3E_z-\Gamma_3H_z-\alpha_3\Delta T,\\
M_y&=B_{12}\varepsilon_x^0+B_{22}\varepsilon_y^0+D_{12}k_x^1+D_{22}k_y^1+F_{12}k_x^3+F_{22}k_y^3-\Phi_4E_z-\Gamma_4H_z-\alpha_4\Delta T,\\
M_{xy}&=B_{66}\gamma_{xy}^0+D_{66}k_{xy}^1+F_{66}k_{xy}^3,\\
P_x&=E_{11}\varepsilon_x^0+E_{12}\varepsilon_y^0+F_{11}k_x^1+F_{12}k_y^1+H_{11}k_x^3+H_{12}k_y^3-\Phi_5E_z-\Gamma_5H_z-\alpha_5\Delta T,\\
P_y&=E_{12}\varepsilon_x^0+E_{22}\varepsilon_y^0+F_{12}k_x^1+F_{22}k_y^1+H_{12}k_x^3+H_{22}k_y^3-\Phi_6E_z-\Gamma_6H_z-\alpha_6\Delta T,\\
P_{xy}&=E_{66}\gamma_{xy}^0+F_{66}k_{xy}^1+H_{66}k_{xy}^3,\\
Q_x&=A_{44}\gamma_{xz}^0+D_{44}k_{xz}^2-\Phi_7E_x-\Gamma_7H_x,\ Q_y=A_{55}\gamma_{yz}^0+D_{55}k_{yz}^2-\Phi_8E_y-\Gamma_8H_y,\\
R_x&=D_{44}\gamma_{xz}^0+F_{44}k_{xz}^2-\Phi_9E_x-\Gamma_9H_x,\ R_y=D_{55}\gamma_{yz}^0+F_{55}k_{yz}^2-\Phi_{10}E_y-\Gamma_{10}H_y,
\end{aligned} \tag{11}$$

in which the detail of coefficients $A_{ij},B_{ij},D_{ij},E_{ij},F_{ij},H_{ij}\,(ij=11,12,22,44,55,66)$; $\Gamma_i,\Phi_i\,(i=\overline{1,10})$; $\alpha_j(j=\overline{1,6})$ are expressed in Appendix B.

The strain components in the middle surface of the auxetic laminated plate are obtained from the first three equations of system Eq. (11) as

$$\begin{aligned}
\varepsilon_x^0&=I_{11}\frac{\partial^2 f}{\partial y^2}-I_{12}\frac{\partial^2 f}{\partial x^2}+I_{13}\frac{\partial\phi_x}{\partial x}+I_{14}\frac{\partial\phi_y}{\partial y}-c_1I_{15}\left(\frac{\partial^2 w}{\partial x^2}+\frac{\partial\phi_x}{\partial x}\right)\\
&\quad-c_1I_{16}\left(\frac{\partial^2 w}{\partial y^2}+\frac{\partial\phi_y}{\partial y}\right)+I_{17}\phi_0+I_{18}\psi_0+I_{19}\Delta T,\\
\varepsilon_y^0&=I_{21}\frac{\partial^2 f}{\partial x^2}-I_{12}\frac{\partial^2 f}{\partial y^2}+I_{23}\frac{\partial\phi_x}{\partial x}+I_{24}\frac{\partial\phi_y}{\partial y}-c_1I_{25}\left(\frac{\partial^2 w}{\partial x^2}+\frac{\partial\phi_x}{\partial x}\right)\\
&\quad-c_1I_{26}\left(\frac{\partial^2 w}{\partial y^2}+\frac{\partial\phi_y}{\partial y}\right)+I_{27}\phi_0+I_{28}\psi_0+I_{29}\Delta T,\\
\gamma_{xy}^0&=-I_{31}\frac{\partial^2 f}{\partial x\partial y}+I_{32}\left(\frac{\partial\phi_x}{\partial y}+\frac{\partial\phi_y}{\partial x}\right)-c_1I_{33}\left(2\frac{\partial^2 w}{\partial x\partial y}+\frac{\partial\phi_x}{\partial y}+\frac{\partial\phi_y}{\partial x}\right),
\end{aligned} \tag{12}$$

where

(13)

and the Airy's stress function $f(x,y,t)$ is defined as

$$N_x=\frac{\partial^2 f}{\partial y^2},\ N_y=\frac{\partial^2 f}{\partial x^2},\ N_{xy}=-\frac{\partial^2 f}{\partial x\partial y}. \tag{14}$$

3.3. Motion equations

Based on the Reddy's higher order shear deformation plate theory and a von Karman-type of kinematic nonlinearity, the nonlinear motion equations of the auxetic laminated plate are [37,38]

$$\frac{\partial N_x}{\partial x}+\frac{\partial N_{xy}}{\partial y}=\bar{j}_1\frac{\partial^2 u}{\partial t^2}+\bar{j}_2\frac{\partial^2\phi_x}{\partial t^2}-\bar{j}_3\frac{\partial^3 w}{\partial t^2\partial x}, \tag{15a}$$

$$\frac{\partial N_{xy}}{\partial x}+\frac{\partial N_y}{\partial y}=\bar{j}_1^*\frac{\partial^2 v}{\partial t^2}+\bar{j}_2^*\frac{\partial^2\phi_y}{\partial t^2}-\bar{j}_3^*\frac{\partial^3 w}{\partial t^2\partial y}, \tag{15b}$$

$$\begin{aligned}
&\frac{\partial Q_x}{\partial x}+\frac{\partial Q_y}{\partial y}-3c_1\left(\frac{\partial R_x}{\partial x}+\frac{\partial R_y}{\partial y}\right)+c_1\left(\frac{\partial^2 P_x}{\partial x^2}+2\frac{\partial^2 P_y}{\partial x\partial y}+\frac{\partial^2 P_y}{\partial y^2}\right)+q+N_x\frac{\partial^2 w}{\partial x^2}\\
&+2N_{xy}\frac{\partial^2 w}{\partial x\partial y}+N_y\frac{\partial^2 w}{\partial y^2}-k_1w+k_2\nabla^2 w=j_1\frac{\partial^2 w}{\partial t^2}+2\varepsilon j_1\frac{\partial w}{\partial t}\\
&+\bar{j}_3\frac{\partial^3 u}{\partial t^2\partial x}+\bar{j}_5\frac{\partial^3\phi_x}{\partial t^2\partial x}+\bar{j}_3^*\frac{\partial^3 v}{\partial t^2\partial y}+\bar{j}_5^*\frac{\partial^3\phi_y}{\partial t^2\partial y}-c_1^2j_7\left(\frac{\partial^4 w}{\partial t^2\partial x^2}+\frac{\partial^4 w}{\partial t^2\partial y^2}\right),
\end{aligned} \tag{15c}$$

$$\frac{\partial M_x}{\partial x}+\frac{\partial M_{xy}}{\partial y}-Q_x+3c_1R_x-c_1\left(\frac{\partial P_x}{\partial x}+\frac{\partial P_{xy}}{\partial y}\right)=\bar{j}_2\frac{\partial^2 u}{\partial t^2}+\bar{j}_4\frac{\partial^2\phi_x}{\partial t^2}-\bar{j}_5\frac{\partial^3 w}{\partial t^2\partial x}, \tag{15d}$$

$$\frac{\partial M_{xy}}{\partial x}+\frac{\partial M_y}{\partial y}-Q_y+3c_1R_y-c_1\left(\frac{\partial P_{xy}}{\partial x}+\frac{\partial P_y}{\partial y}\right)=\bar{j}_2^*\frac{\partial^2 v}{\partial t^2}+\bar{j}_4^*\frac{\partial^2\phi_y}{\partial t^2}-\bar{j}_5^*\frac{\partial^3 w}{\partial t^2\partial y}, \tag{15e}$$

$$\begin{aligned}
&\int_{-h_c/2-h_f}^{h_c/2}\left(\frac{\partial D_x}{\partial x}\cos(\beta z)+\frac{\partial D_y}{\partial y}\cos(\beta z)+D_z\beta\sin(\beta z)\right)dz\\
&+\int_{h_c/2}^{h_c/2+h_f}\left(\frac{\partial D_x}{\partial x}\cos(\beta z)+\frac{\partial D_y}{\partial y}\cos(\beta z)+D_z\beta\sin(\beta z)\right)dz=0,
\end{aligned} \tag{15f}$$

$$\begin{aligned}
&\int_{-h_c/2-h_f}^{h_c/2}\left(\frac{\partial B_x}{\partial x}\cos(\beta z)+\frac{\partial B_y}{\partial y}\cos(\beta z)+B_z\beta\sin(\beta z)\right)dz\\
&+\int_{h_c/2}^{h_c/2+h_f}\left(\frac{\partial B_x}{\partial x}\cos(\beta z)+\frac{\partial B_y}{\partial y}\cos(\beta z)+B_z\beta\sin(\beta z)\right)dz=0,
\end{aligned} \tag{15g}$$

where ε is the viscous damping coefficient, k_1 and k_2 are two

$$\begin{aligned}
&\Delta=A_{11}A_{22}-A_{12}^2,\ I_{11}=\frac{A_{22}}{\Delta},\ I_{12}=\frac{A_{12}}{\Delta},\ I_{13}=\frac{B_{12}A_{12}-B_{11}A_{22}}{\Delta},\ I_{14}=\frac{B_{22}A_{12}-B_{12}A_{22}}{\Delta},\\
&I_{15}=\frac{E_{12}A_{12}-E_{11}A_{22}}{\Delta},\ I_{16}=\frac{E_{22}A_{12}-E_{12}A_{22}}{\Delta},\ I_{17}=2\frac{2e_{32}A_{12}-2e_{31}A_{22}}{\Delta},\\
&I_{18}=2\frac{2q_{32}A_{12}-2q_{31}A_{22}}{\Delta},I_{19}=\frac{-\alpha_2A_{12}+\alpha_1A_{22}}{\Delta},\ I_{21}=\frac{A_{11}}{\Delta},\ I_{23}=\frac{B_{11}A_{12}-B_{12}A_{11}}{\Delta},\\
&I_{24}=\frac{B_{12}A_{12}-B_{22}A_{11}}{\Delta},\ I_{25}=\frac{E_{11}A_{12}-E_{12}A_{11}}{\Delta},\ I_{26}=\frac{E_{12}A_{12}-E_{22}A_{11}}{\Delta},\\
&I_{27}=2\frac{2e_{31}A_{12}-2e_{32}A_{11}}{\Delta},\ I_{28}=2\frac{2q_{31}A_{12}-2q_{32}A_{11}}{\Delta},\\
&I_{29}=\frac{-\alpha_1A_{12}+\alpha_2A_{11}}{\Delta},\ I_{31}=\frac{1}{A_{66}},\ I_{32}=-\frac{B_{66}}{A_{66}},\ I_{33}=-\frac{E_{66}}{A_{66}},
\end{aligned}$$

coefficients of Pasternak-type elastic foundations, q is blast loading and

$$\overline{j_1} = j_1, \overline{j_2} = j_2 - c_1 j_4, \overline{j_3} = c_1 j_4, \overline{j_4} = j_3 - 2c_1 j_5 + c_1^2 j_7,\ \overline{j_5} = c_1 j_5 - c_1^2 j_7,$$

$$(j_1, j_2, j_3, j_4, j_5, j_7) = \int_{-h_f - \frac{h_c}{2}}^{-\frac{h_c}{2}} \rho_f(z)\left(1, z, z^2, z^3, z^4, z^6\right) dz$$
$$+ \int_{-\frac{h_c}{2}}^{\frac{h_c}{2}} \rho_c(z)\left(1, z, z^2, z^3, z^4, z^6\right) dz + \int_{\frac{h_c}{2}}^{\frac{h_c}{2}+h_f} \rho_f(z)\left(1, z, z^2, z^3, z^4, z^6\right) dz. \tag{16}$$

The blast loading is considered as an external pressure uniformly distributed on the surface of the auxetic laminated plate and assumed to depend on time as [4]

$$q(t) = 1.8 Ps_{max}\left(1 - \frac{t}{T_s}\right) exp\left(\frac{-bt}{T_s}\right), \tag{17}$$

where the "1.8″ is parameter which express the effects of a hemi-spherical blast, Ps_{max} is the maximum static over-pressure, b is the parameter controlling the rate of wave amplitude decay and T_s is the parameter characterizing the duration of the blast pulse.

Substituting Eq. (14) into Eqs. (15a) and (15b), the second derivative of the displacement components in $x-$ and $y-$ directions are obtained as

$$\frac{\partial^2 u}{\partial t^2} = -\frac{\overline{j_2}}{\overline{j_1}}\frac{\partial^2 \phi_x}{\partial t^2} + \frac{\overline{j_3}}{\overline{j_1}}\frac{\partial^3 w}{\partial t^2 \partial x}, \tag{18a}$$

$$\frac{\partial^2 v}{\partial t^2} = -\frac{\overline{j_2^*}}{\overline{j_1^*}}\frac{\partial^2 \phi_y}{\partial t^2} + \frac{\overline{j_3^*}}{\overline{j_1^*}}\frac{\partial^3 w}{\partial t^2 \partial y}. \tag{18b}$$

Substituting Eqs. (18a) and (18b) into Eqs. (15c) – (15g), the equations of motion becomes

$$\frac{\partial Q_x}{\partial x} + \frac{\partial Q_y}{\partial y} - 3c_1\left(\frac{\partial R_x}{\partial x} + \frac{\partial R_y}{\partial y}\right) + c_1\left(\frac{\partial^2 P_x}{\partial x^2} + 2\frac{\partial^2 P_{xy}}{\partial x \partial y} + \frac{\partial^2 P_y}{\partial y^2}\right) + \frac{\partial^2 f}{\partial y^2}\frac{\partial^2 w}{\partial x^2}$$
$$-2\frac{\partial^2 f}{\partial x \partial y}\frac{\partial^2 w}{\partial x \partial y} + \frac{\partial^2 f}{\partial x^2}\frac{\partial^2 w}{\partial y^2} + q - k_1 w + k_2 \nabla^2 w \tag{19a}$$

$$= j_1 \frac{\partial^2 w}{\partial t^2} + 2\varepsilon j_1 \frac{\partial w}{\partial t} + \overline{\overline{j_5}}\frac{\partial^3 \phi_x}{\partial t^2 \partial x} + \overline{\overline{j_5^*}}\frac{\partial^3 \phi_y}{\partial t^2 \partial y} + \overline{\overline{j_7}}\frac{\partial^4 w}{\partial t^2 \partial x^2} + \overline{\overline{j_7^*}}\frac{\partial^4 w}{\partial t^2 \partial y^2},$$

$$\frac{\partial M_x}{\partial x} + \frac{\partial M_{xy}}{\partial y} - Q_x + 3c_1 R_x - c_1\left(\frac{\partial P_x}{\partial x} + \frac{\partial P_{xy}}{\partial y}\right) = \overline{\overline{j_3}}\frac{\partial^2 \phi_x}{\partial t^2} - \overline{\overline{j_5}}\frac{\partial^3 w}{\partial t^2 \partial x}, \tag{19b}$$

$$\frac{\partial M_{xy}}{\partial x} + \frac{\partial M_y}{\partial y} - Q_y + 3c_1 R_y - c_1\left(\frac{\partial P_{xy}}{\partial x} + \frac{\partial P_y}{\partial y}\right) = \overline{\overline{j_3^*}}\frac{\partial^2 \phi_y}{\partial t^2} - \overline{\overline{j_5^*}}\frac{\partial^3 w}{\partial t^2 \partial y}, \tag{19c}$$

$$\int_{-h_c/2-h_f}^{h_c/2}\left(\frac{\partial D_x}{\partial x}\cos(\beta z) + \frac{\partial D_y}{\partial y}\cos(\beta z) + D_z \beta \sin(\beta z)\right) dz$$
$$+ \int_{h_c/2}^{h_c/2+h_f}\left(\frac{\partial D_x}{\partial x}\cos(\beta z) + \frac{\partial D_y}{\partial y}\cos(\beta z) + D_z \beta \sin(\beta z)\right) dz = 0, \tag{19d}$$

$$\int_{-h_c/2-h_f}^{h_c/2}\left(\frac{\partial B_x}{\partial x}\cos(\beta z) + \frac{\partial B_y}{\partial y}\cos(\beta z) + B_z \beta \sin(\beta z)\right) dz$$
$$+ \int_{h_c/2}^{h_c/2+h_f}\left(\frac{\partial B_x}{\partial x}\cos(\beta z) + \frac{\partial B_y}{\partial y}\cos(\beta z) + B_z \beta \sin(\beta z)\right) dz = 0, \tag{19e}$$

where

$$\overline{\overline{j_3}} = \overline{j_4} - \left(\overline{j_2}\right)^2 \Big/ \overline{j_1}, \overline{\overline{j_3^*}} = \overline{j_4^*} - \left(\overline{j_2^*}\right)^2 \Big/ \overline{j_1^*}, \overline{\overline{j_3}} = \overline{j_5} - \overline{j_2 j_3} \Big/ \overline{j_1}, \overline{\overline{j_3^*}} = \overline{j_5^*} - \overline{j_2^* j_3^*} \Big/ \overline{j_1^*},$$
$$\overline{\overline{j_3}} = \left(\overline{j_3}\right)^2 \Big/ \overline{j_1} - c_1^2 j_7, \overline{\overline{j_3^*}} = \left(\overline{j_3^*}\right)^2 \Big/ \overline{j_1^*} - c_1^2 j_7. \tag{20}$$

By substituting Eq. (12) into Eq. (11), then the results into Eqs. (19a) – (19e) yields

$$L_{11}(w) + L_{12}(\phi_x) + L_{13}\left(\phi_y\right) + L_{14}(f) + L_{15}(\Phi) + L_{16}(\Psi) + S(w, f)$$
$$+q = j_1 \frac{\partial^2 w}{\partial t^2} + 2\varepsilon j_1 \frac{\partial w}{\partial t} + \overline{\overline{j_5}}\frac{\partial^3 \phi_x}{\partial t^2 \partial x} + \overline{\overline{j_5^*}}\frac{\partial^3 \phi_y}{\partial t^2 \partial y} + \overline{\overline{j_7}}\frac{\partial^4 w}{\partial t^2 \partial x^2} + \overline{\overline{j_7^*}}\frac{\partial^4 w}{\partial t^2 \partial y^2},$$
$$L_{21}(w) + L_{22}(\phi_x) + L_{23}\left(\phi_y\right) + L_{24}(f) + L_{25}(\Phi) + L_{26}(\Psi) = \overline{\overline{j_3}}\frac{\partial^2 \phi_x}{\partial t^2} - \overline{\overline{j_5}}\frac{\partial^3 w}{\partial t^2 \partial x},$$
$$L_{31}(w) + L_{32}(\phi_x) + L_{33}\left(\phi_y\right) + L_{34}(f) + L_{35}(\Phi) + L_{36}(\Psi) = \overline{\overline{j_3^*}}\frac{\partial^2 \phi_y}{\partial t^2} - \overline{\overline{j_5^*}}\frac{\partial^3 w}{\partial t^2 \partial y}, \tag{21}$$

$$\int_{-h_c/2-h_f}^{h_c/2}\left(\frac{\partial D_x}{\partial x}\cos(\beta z) + \frac{\partial D_y}{\partial y}\cos(\beta z) + D_z \beta \sin(\beta z)\right) dz$$
$$+ \int_{h_c/2}^{h_c/2+h_f}\left(\frac{\partial D_x}{\partial x}\cos(\beta z) + \frac{\partial D_y}{\partial y}\cos(\beta z) + D_z \beta \sin(\beta z)\right) dz = 0,$$

$$\int_{-h_c/2-h_f}^{h_c/2}\left(\frac{\partial B_x}{\partial x}\cos(\beta z) + \frac{\partial B_y}{\partial y}\cos(\beta z) + B_z \beta \sin(\beta z)\right) dz$$
$$+ \int_{h_c/2}^{h_c/2+h_f}\left(\frac{\partial B_x}{\partial x}\cos(\beta z) + \frac{\partial B_y}{\partial y}\cos(\beta z) + B_z \beta \sin(\beta z)\right) dz = 0,$$

where the details of operators L_{1i}, L_{2i}, L_{3i} $(i = \overline{1,6})$, S can be found in Appendix C.

For an imperfect auxetic laminated plate, Eq. (21) takes the form of

$$
\begin{aligned}
&L_{11}(w)+L_{12}(\phi_x)+L_{13}(\phi_y)+L_{14}(f)++L_{15}(\Phi)+L_{16}(\Psi)+S(w,f)\\
&+L_{11}^{*}(w^{*})+S^{*}(w^{*},f)+q=j_1\frac{\partial^2 w}{\partial t^2}+2\varepsilon j_1\frac{\partial w}{\partial t}+\bar{\bar{j}}_5\frac{\partial^3\phi_x}{\partial t^2\partial x}+\bar{\bar{j}}_5^{*}\frac{\partial^3\phi_y}{\partial t^2\partial y}+\bar{\bar{j}}_7\frac{\partial^4 w}{\partial t^2\partial x^2}+\bar{\bar{j}}_7^{*}\frac{\partial^4 w}{\partial t^2\partial y^2},\\
&L_{21}(w)+L_{22}(\phi_x)+L_{23}(\phi_y)+L_{24}(f)+L_{21}^{*}(w^{*})+L_{25}(\Phi)+L_{26}(\Psi)=\bar{\bar{j}}_3\frac{\partial^2\phi_x}{\partial t^2}-\bar{\bar{j}}_5\frac{\partial^3 w}{\partial t^2\partial x},\\
&L_{31}(w)+L_{32}(\phi_x)+L_{33}(\phi_y)+L_{34}(f)+L_{31}^{*}(w^{*})+L_{35}(\Phi)+L_{36}(\Psi)=\bar{\bar{j}}_3^{*}\frac{\partial^2\phi_y}{\partial t^2}-\bar{\bar{j}}_5^{*}\frac{\partial^3 w}{\partial t^2\partial y},\\
&\int_{-h_c/2-h_f}^{h_c/2}\left(\frac{\partial D_x}{\partial x}\cos(\beta z)+\frac{\partial D_y}{\partial y}\cos(\beta z)+D_z\beta\sin(\beta z)\right)dz\\
&+\int_{h_c/2}^{h_c/2+h_f}\left(\frac{\partial D_x}{\partial x}\cos(\beta z)+\frac{\partial D_y}{\partial y}\cos(\beta z)+D_z\beta\sin(\beta z)\right)dz=0,\\
&\int_{-h_c/2-h_f}^{h_c/2}\left(\frac{\partial B_x}{\partial x}\cos(\beta z)+\frac{\partial B_y}{\partial y}\cos(\beta z)+B_z\beta\sin(\beta z)\right)dz\\
&+\int_{h_c/2}^{h_c/2+h_f}\left(\frac{\partial B_x}{\partial x}\cos(\beta z)+\frac{\partial B_y}{\partial y}\cos(\beta z)+B_z\beta\sin(\beta z)\right)dz=0,
\end{aligned}
\tag{22}
$$

where the function $w^{*}(x,y)$ presents an initial geometrical imperfection which is assumed to be smaller than the deflection of the auxetic laminated plate and

$$
L_{11}^{*}(w^{*})=X_{11}\frac{\partial^2 w^{*}}{\partial x^2}+X_{12}\frac{\partial^2 w^{*}}{\partial y^2},S^{*}(w^{*},f)=\frac{\partial^2 f}{\partial y^2}\frac{\partial^2 w^{*}}{\partial x^2}-2\frac{\partial^2 f}{\partial x\partial y}\frac{\partial^2 w^{*}}{\partial x\partial y}+\frac{\partial^2 f}{\partial x^2}\frac{\partial^2 w^{*}}{\partial y^2},
$$
$$
L_{21}^{*}(w^{*})=X_{21}\frac{\partial w^{*}}{\partial x},L_{31}^{*}(w^{*})=X_{31}\frac{\partial w^{*}}{\partial y}.
\tag{23}
$$

From Eq. (3), the strain components by the following geometrical compatibility equation [37,38]

$$
\frac{\partial^2\varepsilon_x^0}{\partial y^2}+\frac{\partial^2\varepsilon_y^0}{\partial x^2}-\frac{\partial^2\gamma_{xy}^0}{\partial x\partial y}=\frac{\partial^2 w}{\partial x\partial y}^2-\frac{\partial^2 w}{\partial x^2}\frac{\partial^2 w}{\partial y^2}+2\frac{\partial^2 w}{\partial x\partial y}\frac{\partial^2 w^{*}}{\partial x\partial y}-\frac{\partial^2 w}{\partial x^2}\frac{\partial^2 w^{*}}{\partial y^2}-\frac{\partial^2 w}{\partial y^2}\frac{\partial^2 w^{*}}{\partial x^2}.
\tag{24}
$$

Substituting Eq. (12) into Eq. (24), the compatibility equation of the imperfect auxetic laminated plate are rewritten as

$$
\begin{aligned}
&I_{21}\frac{\partial^4 f}{\partial x^4}+I_{11}\frac{\partial^4 f}{\partial y^4}+J_1\frac{\partial^4 f}{\partial x^2\partial y^2}+J_2\frac{\partial^3\phi_x}{\partial x^3}+J_3\frac{\partial^3\phi_x}{\partial x\partial y^2}+J_4\frac{\partial^3\phi_y}{\partial y^3}\\
&+J_5\frac{\partial^3\phi_y}{\partial y\partial x^2}-c_1I_{25}\frac{\partial^4 w}{\partial x^4}-c_1I_{16}\frac{\partial^4 w}{\partial y^4}+J_6\frac{\partial^4 w}{\partial x^2\partial y^2}\\
&-\left(\frac{\partial^2 w}{\partial x\partial y}^2-\frac{\partial^2 w}{\partial x^2}\frac{\partial^2 w}{\partial y^2}+2\frac{\partial^2 w}{\partial x\partial y}\frac{\partial^2 w^{*}}{\partial x\partial y}-\frac{\partial^2 w}{\partial x^2}\frac{\partial^2 w^{*}}{\partial y^2}-\frac{\partial^2 w}{\partial y^2}\frac{\partial^2 w^{*}}{\partial x^2}\right)=0,
\end{aligned}
\tag{25}
$$

in which

$$
\begin{aligned}
&J_1=I_{31}-2I_{12},\ J_2=I_{23}-c_1I_{25},\ J_3=I_{13}-c_1I_{15}-I_{32}+c_1I_{33},\\
&J_4=I_{14}-c_1I_{16},\ J_5=I_{24}-c_1I_{26}-I_{32}+c_1I_{33},\ J_6=-c_1I_{15}-c_1I_{26}+2c_1I_{33}.
\end{aligned}
\tag{26}
$$

Two nonlinear differential equations (22) and (25) are used to determine the vibration characteristics of imperfect auxetic laminated plate subjected to the combination of mechanical, thermal, electric and magnetic loadings based on the Reddy's higher order shear deformation plate theory.

3.4. Solutions procedure

Simply supported boundary conditions of the auxetic laminated plate are considered in this study in which four edges are immovable in the $x-$ and $y-$ directions. The boundary conditions can be expressed as

$$
\begin{aligned}
&w=u=\phi_y=M_x=N_{xy}=0,\ N_x=N_{x0}\ at\ x=0,a,\\
&w=v=\phi_x=M_y=N_{xy}=0,\ N_y=N_{y0}\ at\ y=0,b,
\end{aligned}
\tag{27}
$$

where $N_{x0},\ N_{y0}$ are fictitious compressive edge loads at four edges.

The approximate solutions of nonlinear system of differential equations (22) and (25) are driven as

$$
\begin{aligned}
&w(x,y,t)=W(t)sin\lambda_m xsin\delta_n y,\\
&\Phi(x,y,t)=\phi(t)sin\lambda_m xsin\delta_n y,\\
&\Psi(x,y,t)=\psi(t)sin\lambda_m xsin\delta_n y,\\
&\phi_x(x,y,t)=\Phi_x(t)cos\lambda_m xsin\delta_n y,\\
&\phi_y(x,y,t)=\Phi_y(t)sin\lambda_m xcos\delta_n y,
\end{aligned}
\tag{28}
$$

where $\lambda_m=m\pi/a,\ \delta_n=n\pi/b$ with m,n are odd natural numbers; $W(t),\ \Phi_x(t),\ \Phi_y(t),\ \phi(t)$ and $\psi(t)$ refer to maximum values of solutions which are time – dependent functions.

In order to consider the greatest effect of initial imperfection, function w^{*} is assumed to have the similar form of the deflection as

$$
w^{*}(x,y,t)=\mu hsin\lambda_m xsin\delta_n y,
\tag{29}
$$

with μ $(0\leqslant\mu\leqslant 1)$ is initial imperfection parameter.

Substituting Eqs. (28) and (29) into Eq. (25) and balancing both sides of the obtained equation, the Airy's stress function can be found as follows

$$
\begin{aligned}
f(x,y,t)=&T_1(t)cos2\lambda_m x+T_2(t)cos2\delta_n y+T_3(t)sin\lambda_m xsin\delta_n y+\\
&\frac{1}{2}N_{y0}x^2+\frac{1}{2}N_{x0}y^2,
\end{aligned}
\tag{30}
$$

in which

$$
\begin{aligned}
&T_1=\frac{\delta_n^2}{32I_{21}\lambda_m^2}W(W+2\mu h),T_2=\frac{\lambda_m^2}{32I_{11}\delta_n^2}W(W+2\mu h),\\
&T_3=Q_1W+Q_2\Phi_x+Q_3\Phi_y,
\end{aligned}
\tag{31}
$$

with

$$
\begin{aligned}
&Q_1=\frac{c_1I_{25}\lambda_m^4+c_1I_{16}\delta_n^4-J_6\lambda_m^2\delta_n^2}{I_{21}\lambda_m^4+J_1\lambda_m^2\delta_n^2+I_{11}\delta_n^4},\\
&Q_2=\frac{-(J_2\lambda_m^3+J_3\lambda_m\delta_n^2)}{I_{21}\lambda_m^4+J_1\lambda_m^2\delta_n^2+I_{11}\delta_n^4},\ Q_3=\frac{-(J_4\delta_n^3+J_5\lambda_m^2\delta_n)}{I_{21}\lambda_m^4+J_1\lambda_m^2\delta_n^2+I_{11}\delta_n^4}.
\end{aligned}
\tag{32}
$$

By substituting Eqs. (28) – (30) into Eq. (22) and applying Galerkin method in the domain $0\leqslant x\leqslant a$ and $0\leqslant y\leqslant b$ to the resulting equation, we obtain the nonlinear system motion equations as

$$\begin{aligned}
&l_{11}W+l_{12}\Phi_x+l_{13}\Phi_y+l_{14}(W+\mu h)\Phi_x+l_{15}(W+\mu h)\Phi_y+l_{16}\phi+l_{17}\psi\\
&\quad+\left[n_1-N_{x0}\lambda_m^2-N_{y0}\delta_n^2\right](W+\mu h)+n_2W(W+\mu h)\\
&\quad+n_3W(W+2\mu h)+n_4W(W+\mu h)(W+2\mu h)\\
&\quad+n_5q=j_0\frac{\partial^2W}{\partial t^2}+2\varepsilon j_1\frac{\partial W}{\partial t}-\lambda_m\bar{\bar{j}}_5\frac{\partial^2\Phi_x}{\partial t^2}-\delta_n\bar{\bar{j}}_5^*\frac{\partial^2\Phi_y}{\partial t^2},\\
&l_{21}W+l_{22}\Phi_x+l_{23}\Phi_y+l_{24}\phi+l_{25}\psi+n_6(W+\mu h)\\
&\quad+n_7W(W+2\mu h)=\bar{\bar{j}}_3\frac{\partial^2\Phi_x}{\partial t^2}-\lambda_m\bar{\bar{j}}_5\frac{\partial^2W}{\partial t^2},\\
&l_{31}W+l_{32}\Phi_x+l_{33}\Phi_y+l_{34}\phi+l_{35}\psi+n_8(W+\mu h)\\
&\quad+n_9W(W+2\mu h)=\bar{\bar{j}}_3^*\frac{\partial^2\Phi_y}{\partial t^2}-\delta_n\bar{\bar{j}}_5^*\frac{\partial^2W}{\partial t^2},\\
&l_{41}W+l_{42}\Phi_x+l_{43}\Phi_y+l_{44}\phi+l_{45}\psi=0,\\
&l_{51}W+l_{52}\Phi_x+l_{53}\Phi_y+l_{54}\phi+l_{55}\psi=0,
\end{aligned}\tag{33}$$

where the detail of coefficients $l_{1i}(i=\overline{1,7}),l_{jk}(j=\overline{2,3,4,5},k=\overline{1,5})$, $n_m(m=\overline{1,9})$ are expressed in Appendix D.

3.5. Vibration behaviors

The immovability conditions (i.e. $u=0$ on $x=0,a$ and $v=0$ on $y=0,b$) can be satisfied on the average sense as follows [27]

$$\int_0^b\int_0^a\frac{\partial u}{\partial x}dxdy=0,\quad\int_0^a\int_0^b\frac{\partial v}{\partial x}dydx=0.\tag{34}$$

The following expressions are obtained from Eqs. (3) and (12) as

$$\begin{aligned}
&\frac{\partial u}{\partial x}=I_{11}\frac{\partial^2f}{\partial y^2}-I_{12}\frac{\partial^2f}{\partial x^2}+I_{13}\frac{\partial\phi_x}{\partial x}+I_{14}\frac{\partial\phi_y}{\partial y}-c_1I_{15}\left(\frac{\partial^2w}{\partial x^2}+\frac{\partial\phi_x}{\partial x}\right)\\
&-c_1I_{16}\left(\frac{\partial^2w}{\partial y^2}+\frac{\partial\phi_y}{\partial y}\right)+I_{17}\phi_0+I_{18}\psi_0+I_{19}\Delta T-\frac{1}{2}\left(\frac{\partial w}{\partial x}\right)^2-\frac{\partial w}{\partial x}\frac{\partial w^*}{\partial x},\\
&\frac{\partial v}{\partial y}=I_{21}\frac{\partial^2f}{\partial x^2}-I_{12}\frac{\partial^2f}{\partial y^2}+I_{23}\frac{\partial\phi_x}{\partial x}+I_{24}\frac{\partial\phi_y}{\partial y}-c_1I_{25}\left(\frac{\partial^2w}{\partial x^2}+\frac{\partial\phi_x}{\partial x}\right)\\
&-c_1I_{26}\left(\frac{\partial^2w}{\partial y^2}+\frac{\partial\phi_y}{\partial y}\right)+I_{27}\phi_0+I_{28}\psi_0+I_{29}\Delta T-\frac{1}{2}\left(\frac{\partial w}{\partial y}\right)^2-\frac{\partial w}{\partial y}\frac{\partial w^*}{\partial y}.
\end{aligned}\tag{35}$$

By substituting Eqs. (28) – (30) into Eq. (35), then the results into Eq. (34), the fictitious compressive edge loads are obtained as

$$\begin{aligned}
N_{x0}&=g_1W+g_4(W+2\mu h)W+g_2\Phi_x+g_3\Phi_y+g_5\phi_0+g_6\psi_0+g_7\Delta T,\\
N_{y0}&=f_1W+f_4(W+2\mu h)W+f_2\Phi_x+f_3\Phi_y+f_5\phi_0+f_6\psi_0+f_7\Delta T,
\end{aligned}\tag{36}$$

where the details of coefficients $g_i\,(i=\overline{1,7})$ and $f_j\,(j=\overline{1,7})$ are expressed in Appendix E.

Substituting Eq. (36) into Eq. (33), one has

$$\begin{aligned}
&l_{11}W+l_{12}\Phi_x+l_{13}\Phi_y+l_{14}^1(W+\mu h)\Phi_x+l_{15}^1(W+\mu h)\Phi_y+n_1^1(W+\mu h)+l_{16}\phi+l_{17}\psi\\
&\quad+n_2^1W(W+\mu h)+n_3W(W+2\mu h)+n_4^1W(W+\mu h)(W+2\mu h)\\
&\quad+n_5q=j_0\frac{\partial^2W}{\partial t^2}+2\varepsilon j_1\frac{\partial W}{\partial t}-\lambda_m\bar{\bar{j}}_5\frac{\partial^2\Phi_x}{\partial t^2}-\delta_n\bar{\bar{j}}_5^*\frac{\partial^2\Phi_y}{\partial t^2},\\
&l_{21}W+l_{22}\Phi_x+l_{23}\Phi_y+l_{24}\phi+l_{25}\psi+n_6(W+\mu h)\\
&\quad+n_7W(W+2\mu h)=\bar{\bar{j}}_3\frac{\partial^2\Phi_x}{\partial t^2}-\lambda_m\bar{\bar{j}}_5\frac{\partial^2W}{\partial t^2},\\
&l_{31}W+l_{32}\Phi_x+l_{33}\Phi_y+l_{34}\phi+l_{35}\psi+n_8(W+\mu h)\\
&\quad+n_9W(W+2\mu h)=\bar{\bar{j}}_3^*\frac{\partial^2\Phi_y}{\partial t^2}-\delta_n\bar{\bar{j}}_5^*\frac{\partial^2W}{\partial t^2},\\
&l_{41}W+l_{42}\Phi_x+l_{43}\Phi_y+l_{44}\phi+l_{45}\psi=0,\\
&l_{51}W+l_{52}\Phi_x+l_{53}\Phi_y+l_{54}\phi+l_{55}\psi=0,
\end{aligned}\tag{37}$$

in which

$$\begin{aligned}
&l_{14}^1=\left(l_{14}-\lambda_m^2g_2-\delta_n^2f_2\right),l_{15}^1=\left(l_{15}-\lambda_m^2g_3-\delta_n^2f_3\right),\\
&\quad n_1^1=n_1-\left(\lambda_m^2g_5+\delta_n^2f_5\right)\phi_0-\left(\lambda_m^2g_6+\delta_n^2f_6\right)\psi_0\\
&\qquad-\left(\lambda_m^2g_7+\delta_n^2f_7\right)\Delta T,\\
&n_2^1=\left(n_2-\lambda_m^2g_1-\delta_n^2f_1\right),n_4^1=\left(n_4-\lambda_m^2g_4-\delta_n^2f_4\right),
\end{aligned}\tag{38}$$

Table 2
Comparison of natural frequencies (Hz) of the sandwich composite plates with auxetic honeycomb core layer with $h=0.1m,\ h_c/h_f=1.5,\ t/l=0.01385,\ a=b,a=20h,\ \theta=-55^0$.

(k_1,k_2)		$d/l=0.5$	$d/l=1$	$d/l=2$	$d/l=4$
(0,0)	Tran et al. [19]	158.6420	142.8576	150.7676	151.7532
	Present	159.2772	143.2607	151.2831	152.2833
(0.1,0)	Tran et al. [19]	206.6414	185.979	196.3308	197.6211
	Present	207.1110	186.2845	196.7162	198.0167
(0.1,0.05)	Tran et al. [19]	293.6156	264.1513	278.9102	280.7500
	Present	293.4928	263.9799	278.7625	280.6054

By collecting the electric and magnetic potentials amplitude from the last two equations of system Eq. (37), then substituting the obtained equations into the first three equations gives

$$\begin{aligned}
&l_{11}^1W+l_{12}^1\Phi_x+l_{13}^1\Phi_y+l_{14}^1(W+\mu h)\Phi_x+l_{15}^1(W+\mu h)\Phi_y+n_1^1(W+\mu h)\\
&\quad+n_2^1W(W+\mu h)+n_3W(W+2\mu h)+n_4^1W(W+\mu h)(W+2\mu h)\\
&\quad+n_5q=j_0\frac{\partial^2W}{\partial t^2}+2\varepsilon j_1\frac{\partial W}{\partial t}-\lambda_m\bar{\bar{j}}_5\frac{\partial^2\Phi_x}{\partial t^2}-\delta_n\bar{\bar{j}}_5^*\frac{\partial^2\Phi_y}{\partial t^2},\\
&l_{21}^1W+l_{22}^1\Phi_x+l_{23}^1\Phi_y+n_6(W+\mu h)+n_7W(W+2\mu h)=\bar{\bar{j}}_3\frac{\partial^2\Phi_x}{\partial t^2}-\lambda_m\bar{\bar{j}}_5\frac{\partial^2W}{\partial t^2},\\
&l_{31}^1W+l_{32}^1\Phi_x+l_{33}^1\Phi_y+n_8(W+\mu h)+n_9W(W+2\mu h)=\bar{\bar{j}}_3^*\frac{\partial^2\Phi_y}{\partial t^2}-\delta_n\bar{\bar{j}}_5^*\frac{\partial^2W}{\partial t^2},
\end{aligned}\tag{39}$$

where the detail of coefficients $l_{jk}^1(j=\overline{1,3},k=\overline{1,3})$ are given in Appendix F.

Eq. (39) is used to investigate the nonlinear vibration characteristics of the auxetic laminated plate on elastic foundations in thermal environment by using Runge-Kutta method. The initial conditions are taken to be $W(0)=0,\ \frac{dW}{dt}(0)=0,\ \Phi_x(0)=0,\ \frac{d\Phi_x}{dt}(0)=0,\ \Phi_y(0)=0,\ \frac{d\Phi_y}{dt}(0)=0$.

For linear free vibration of the auxetic laminated plate, the viscous damping and nonlinear terms are not considered and the loading is considered as zero. The natural frequency of the perfect auxetic laminated plate is given by

Table 3
Comparison of non-dimensional frequencies $\Omega = \omega_L a/\sqrt{c_0/\rho_0}$ of laminated magneto-electro-elastic plates.

Mode		$BaTiO_3/CoFe_2O_4/BaTiO_3$	$CoFe_2O_4/BaTiO_3/CoFe_2O_4$
1	Chen et al. [31]	0.9652	1.0672
	Vinyas et al. [25]	0.9636	1.0623
	Present	0.9392	1.0522
	Maximum error	2.77%	1.43%
2	Chen et al. [31]	1.8556	1.9598
	Vinyas et al. [25]	1.8416	1.973
	Present	1.8894	2.0301
	Maximum error	2.60%	3.59%

$$\begin{vmatrix} l_{11}^1 + n_1^1 + j_0\omega^2 & l_{12}^1 - \lambda_m \bar{\bar{j}}_5 \omega^2 & l_{13}^1 - \delta_n \bar{\bar{j}}_5^* \omega^2 \\ l_{21}^1 + n_6 - \lambda_m \bar{\bar{j}}_5 \omega^2 & l_{22}^1 + \bar{\bar{j}}_3 \omega^2 & l_{23}^1 \\ l_{31}^1 + n_8 - \delta_n \bar{\bar{j}}_5^* \omega^2 & l_{32}^1 & l_{33}^1 + \bar{\bar{j}}_3^* \omega^2 \end{vmatrix} = 0. \tag{40}$$

Let consider the inertial forces caused by the rotation angles as small values and be zero, Eq. (39) becomes

$$\begin{aligned} & l_{11}^1 W + l_{12}^1 \Phi_x + l_{13}^1 \Phi_y + l_{14}^1 (W + \mu h)\Phi_x + l_{15}^1 (W + \mu h)\Phi_y + n_1^1 (W + \mu h) \\ & \quad + n_2^1 W(W + \mu h) + n_3 W(W + 2\mu h) + n_4^1 W(W + \mu h)(W + 2\mu h) \\ & \quad + n_5 q = j_0 \frac{\partial^2 W}{\partial t^2} + 2\varepsilon j_1 \frac{\partial W}{\partial t}, \\ & l_{21}^1 W + l_{22}^1 \Phi_x + l_{23}^1 \Phi_y + n_6 (W + \mu h) + n_7 W(W + 2\mu h) = -\lambda_m \bar{\bar{j}}_5 \frac{\partial^2 W}{\partial t^2}, \\ & l_{31}^1 W + l_{32}^1 \Phi_x + l_{33}^1 \Phi_y + n_8 (W + \mu h) + n_9 W(W + 2\mu h) = -\delta_n \bar{\bar{j}}_5^* \frac{\partial^2 W}{\partial t^2}. \end{aligned} \tag{41}$$

Besides, the uniformly distributed transverse loading is assumed to be in harmonic form as $q = Q sin\Omega t$ in which Q is the amplitude and Ω is the frequency. By substituting the expression of Φ_x and Φ_y which are obtained from the second and third equations of system Eq. (41) into the first equation, one has

$$\begin{aligned} & \left[\bar{j}_0 - j_0^*(W + \mu h)\right] \frac{d^2 W}{dt^2} + 2\varepsilon j_1 \frac{dW}{dt} - b_{11} W - b_{12}(W + \mu h) \\ & - b_{13} W(W + \mu h) - b_{14} W(W + 2\mu h) - b_{15}(W + \mu h)^2 \\ & \quad - b_{16} W(W + \mu h)(W + 2\mu h) = n_5 Q sin\Omega t, \end{aligned} \tag{42}$$

where the details of coefficients $\bar{j}_0$, j_0^* and $b_{1i} (i = \overline{1,6})$ may be found in Appendix G.

For the perfect auxetic laminated plate, Eq. (42) can be rewritten as the following expression

Table 4
Comparison of nonlinear to linear frequency ratios ω_{NL}/ω_L for an isotropic square plate ($a/b = 1$, $b/h = 10$, $\nu = 0.3$).

Source	ξ/h				
	0.2	0.4	0.6	0.8	1
Singh et al. [33]	1.023	1.090	1.192	1.321	1.468
Chen and Doong [34]	1.024	1.091	1.192	1.324	1.467
Bhimaraddi [35]	1.0206	1.0802	1.1728	1.2913	1.4293
Wang and Shen [36]	1.0206	1.0802	1.1728	1.2912	1.4293
Present	1.02064	1.08021	1.17278	1.29128	1.42927

Table 5
Effects of vibration modes (m, n) , elastic foundations coefficients and the inclined angle θ on the natural frequencies of the auxetic laminated plate with magneto-electro-elastic face sheets with $a/b = 1$, $b/h = 20$, $h = 0.05\,m$, $h_c/h_f = 8$, $\Delta T = 0$, $\phi_0 = 400\ V$, $\psi_0 = 200\,A$, $t/l = 0.0138571$, $d/l = 2$.

(m, n)	$k_1,\ k_2$	θ			
		30^0	45^0	60^0	75^0
(1, 1)	(0, 0)	1.9689	1.9634	1.9456	1.8786
(1, 2)	(0, 0)	4.2531	4.2940	4.3477	4.3553
(2, 1)	(0, 0)	4.2386	4.2157	4.1505	3.9623
(2, 2)	(0, 0)	6.0667	6.0978	6.1187	6.0409
(1, 1)	(0.1, 0.02)	3.5240	3.5008	3.4510	3.3068
(1, 2)	(0.1, 0.02)	6.0680	6.0711	6.0591	5.9331
(2, 1)	(0.1, 0.02)	6.0578	6.0163	5.9198	5.6519
(2, 2)	(0.1, 0.02)	8.1062	8.0999	8.0576	7.8452

Table 6
Effects of temperature increment ΔT , ratios a/b and h_c/h_f on the natural frequencies of the auxetic laminated plate with magneto-electro-elastic face sheets with $b/h = 20$, $h = 0.05\,m$, $\phi_0 = 400\ V$, $\psi_0 = 200\ A$, $t/l = 0.0138571$, $\theta = 30^0$, $d/l = 2$.

a/b	h_c/h_f	$\Delta T\,(K)$			
		0	50	100	200
0.5	4	5.6617	5.5997	5.5370	5.4094
1		3.0195	2.9732	2.9261	2.8297
1.5		2.4847	2.4441	2.4028	2.3179
0.5	6	5.8777	5.8173	5.7564	5.6325
1		3.2934	3.2511	3.2084	3.1211
1.5		2.7468	2.7103	2.6734	2.5979
0.5	8	6.0578	5.9982	5.9379	5.8154
1		3.5240	3.4846	3.4448	3.3636
1.5		2.9696	2.9360	2.9021	2.8330

$$\begin{aligned} & \left(\bar{j}_0 - j_0^* W\right) \frac{d^2 W}{dt^2} + 2\varepsilon j_1 \frac{dW}{dt} - (b_{11} + b_{12}) W \\ & - (b_{13} + b_{14} + b_{15}) W^2 - b_{16} W^3 = n_5 Q sin\Omega t. \end{aligned} \tag{43}$$

The coefficient j_0^* in Eq. (43) may be ignored because it is considered as small value. Then, Eq. (43) can be written as follows

$$\begin{aligned} & \frac{d^2 W}{dt^2} + \frac{2\varepsilon j_1}{\bar{j}_0} \frac{dW}{dt} - \frac{(b_{11} + b_{12})}{\bar{j}_0} W \\ & - \frac{(b_{13} + b_{14} + b_{15})}{\bar{j}_0} W^2 - \frac{b_{16}}{\bar{j}_0} W^3 = \frac{n_5}{\bar{j}_0} Q sin\Omega t. \end{aligned} \tag{44}$$

The nonlinear free vibration frequency of the auxetic laminated plate can be given based on Eq. (44) as

Table 7
Effects of electric and magnetic potentials and ratio b/h on the natural frequencies of the auxetic laminated plate with magneto-electro-elastic face sheets with $\Delta T = 0$, $k_1 = 0.1\,GPa/m$, $k_2 = 0.02\,GPa.m$.

b/h	$\psi_0\,(A)$	$\phi_0\,(V)$				
		−800	−400	0	400	800
10	−200	8.0866	8.0854	8.0843	8.0831	8.0820
	0	8.0981	8.0969	8.0958	8.0947	8.0935
	200	8.1096	8.1084	8.1073	8.1062	8.1050
15	−200	4.9066	4.9057	4.9049	4.9041	4.9032
	0	4.9150	4.9142	4.9133	4.9125	4.9117
	200	4.9235	4.9226	4.9218	4.9209	4.9201
20	−200	3.5127	3.5120	3.5114	3.5107	3.5101
	0	3.5194	3.5187	3.5180	3.5174	3.5167
	200	3.5260	3.5253	3.5247	3.5240	3.5234

$$\omega_L = \sqrt{-\frac{(b_{11}+b_{12})}{\overline{j_0}}}. \tag{45}$$

By introducing four coefficients $\overline{j_0^*} = j_1/j_0,\ M = -(b_{13}+b_{14}+b_{15})/(b_{11}+b_{12}),\ \ N = b_{16}/(b_{11}+b_{12})$ and $P = n_5 Q/j_0$, Eq. (44) may be expressed as follows

$$\frac{d^2W}{dt^2} + 2\varepsilon\overline{j_0^*}\frac{dW}{dt} + \omega_L^2\left(W - MW^2 + NW^3\right) - Psin\Omega t = 0, \tag{46}$$

The deflection amplitude is assumed to be the form of $W(t) = \xi sin(\omega t)$. By substituting this form into Eq. (46), the relationship between frequency and amplitude of nonlinear free vibration is determined as

$$\omega_{NL}^2 - 2\varepsilon\overline{j_0^*}\frac{2\omega_{NL}}{\pi} - \omega_L^2\left(1 - M\xi\frac{8}{3\pi} + N\xi^2\frac{3}{4}\right) = 0. \tag{47}$$

where ω_{NL} is nonlinear frequency and ξ is amplitude of free vibration. When the viscous damping is assumed to be zero, Eq. (47) becomes

$$\omega_{NL} = \omega_L\left(1 - M\xi\frac{8}{3\pi} + N\xi^2\frac{3}{4}\right)^{\frac{1}{2}}. \tag{48}$$

4. Results and discussion

4.1. Validation

For the first comparison study to verify the accuracy and reliability of present theory and calculations, the natural frequencies (Hz) of the sandwich composite plates with auxetic honeycomb core layer and isotropic aluminium face sheets on Pasternak-type elastic foundations are considered. For two face sheets, the thickness is the same and the material properties are $E = 69\,GPa,\ \nu = 0.33$ and $\rho = 200\,kg/m^3$. The geometry parameters of single unit cell of auxetic core layer are $t/l = 0.01385,\ \ \theta = -55^0$. The present numerical results are compared with ones of Tran et al. [19] based on Mindlin plate theory and finite element method. Results of this comparison are provided in Table 2 with various values of elastic foundations coefficients and geometrical parameter h/l of auxetic core layer. It is found that the present results are in close agreement with the available data of Tran et al. [19].

For the second verification which is shown in Table 3, the non-dimensional frequencies $\Omega = \omega_L a/\sqrt{c_0/\rho_0}$ of laminated magneto-electro-elastic plates are in which c_0 and ρ_0 are the maximum values of elastic constants and mass densities of Barium Titanate and Cobalt Ferric oxide are considered. Two cases of stacking sequences of piezo-electric and magnetostrictive layers including $BaTiO_3/\,CoFe_2O_4/BaTiO_3$ and $CoFe_2O_4/BaTiO_3/\,CoFe_2O_4$ are mentioned. The present results are compared with numerical results of Chen [31] which are obtained based on the state-vector approach and the finite element results of Vinyas [25] according to Reddy's higher order shear deformation plate theory. The maximum error is 3.59%, which shows the good agreement between our results and available results in the open literature.

For the third comparison study, the values of nonlinear to linear frequency ratios ω_{NL}/ω_L for an isotropic square plate with immovable edge condition are calculated and compared with theoretical results of Singh et al. [33], the average stress method results of Chen and Doong [34], the numerical results of Bhimaraddi [35] using the parabolic shear deformation plate theory and Wang and Shen [36] based on Reddy's higher order shear deformation plate theory. The geometrical and material parameters are taken to be $a/b = 1,\ \ b/h = 10,\ \ \nu = 0.3$. Again, the comparison results from Table 4 show the reliability of present results.

4.2. Parametric studies

Table 5 indicates the effect of vibration modes (m, n) , elastic foundations coefficients $k_1\ (GPa/m),\ \ k_2\ (GPa.m)$ and the inclined angle θ of unit cells on the natural frequency $\left(\times 10^3\,s^{-1}\right)$ of the auxetic laminated plate with magneto-electro-elastic face sheets. Two values of elastic foundations coefficients $(k_1,\ k_2) = (0, 0),\ (0.1,\ 0.02)$ and four values of the inclined angle $\theta = (30^0,\ 45^0,\ 60^0,\ 75^0)$ are considered. As can be seen, the value of the natural frequency of the auxetic laminated plate decreases when the inclined angle increases. The most possible reason is that the stiffness of auxetic core layer decreases when the inclined angle increases, which will result in the reduction of the natural frequency of the auxetic laminated plate. Besides, the value of natural frequency increases considerably when the values of two coefficients of elastic foundations increase. Clearly, the structural stiffness is enhanced by the support of elastic foundations, which leads to the rise of natural frequency. The results from Table 5 also show that an increase of vibration modes results in a strong rise of the natural frequency of auxetic laminated plate.

Table 6 shows the effects of temperature increment ΔT, the plate length to width ratio a/b and the core to face sheet thickness ratio h_c/h_f on the natural frequencies $\left(\times 10^3\,s^{-1}\right)$ of the auxetic laminated plate with magneto-electro-elastic face sheets. The elastic foundations coefficients are chosen to be $k_1 = 0.1\ GPa/m$ and $k_2 = 0.02\,GPa.m$. It is found that the natural frequency of the laminated plate is decreased with increasing temperature increment. One reason is that the structural stiffness decreases when the temperature increment increases. Further, two geometrical parameters have significant effect on the natural frequencies of the auxetic laminated plate. The natural frequency increases by increasing h_c/h_f ratio or decreasing a/b ratio.

The effects of electric and magnetic potentials $\phi_0\ (V)$ and $\psi_0\ (A)$ as well as the plate width to thickness ratio b/h on the natural frequencies $\left(\times 10^3\,s^{-1}\right)$ of the auxetic laminated plate with magneto-electro-elastic face sheets are given in Table 7. The geometrical parameters are taken to be $a/b = 1,\ h_c/h_f = 8,\ b/h = 20,\ h = 0.05\,m$. As can be observed, the natural frequency changes slightly when the electric and magnetic potentials increase. While a decrease of electric potential results in a rise of the natural frequency, the natural frequency decreases due to the decrease of magnetic potential. The reason of such trend is that, as the electric potential increases or the magnetic potential decreases, the structural stiffness decreases, which leads to lower natural frequency. Moreover, the natural frequency is reduced with rising ratio b/h . This is due to the decrease of elasticity modulus of the auxetic laminated plate when ratio b/h increases.

Table 8 illustrates the effects of temperature increment $\Delta T\,(= 0,\ 50\,K,\ 100K)$ and the plate width to thickness ratio $b/h\ (= 15,\ 20,\ 25)$ on the nonlinear to linear frequency ratio ω_{NL}/ω_L of the auxetic laminated plate with magneto-electro-elastic face sheets. The plate length to width ratio is chosen as $a/b = 1$ and two elastic foundations coefficients are taken to be $k_1 = 0.1\,GPa/m,\ k_2 = 0.02\,GPa.m$. It is easy to see that the frequency ratio increases significantly as the temperature increment ΔT is increased. The possible reason for this trend is that the stiffness and

Table 8
Effects of temperature increment ΔT and ratio b/h on the nonlinear to linear frequency ratio ω_{NL}/ω_L of the auxetic laminated plate with magneto-electro-elastic face sheets with $h = 0.05\,m,\ h_c/h_f = 8,\ t/l = 0.0138571,\ \theta = 30^0,\ d/l = 2$.

$\Delta T\,(K)$	b/h	ξ/h				
		0.2	0.4	0.6	0.8	1
0	15	1.010447	1.041161	1.090429	1.155882	1.234949
	20	1.005624	1.022309	1.049529	1.086491	1.132243
	25	1.003477	1.013837	1.030872	1.054258	1.083585
50	15	1.010639	1.041905	1.092026	1.15856	1.238863
	20	1.005742	1.022774	1.050547	1.08824	1.134863
	25	1.003556	1.014148	1.031560	1.055455	1.085403
100	15	1.010838	1.042676	1.093682	1.161333	1.242914
	20	1.005865	1.023259	1.051609	1.090061	1.137592
	25	1.003638	1.014474	1.032280	1.056705	1.087303

Table 9

Effects of magnetic and electric potentials ψ_0 and ϕ_0 on the nonlinear to linear frequency ratio ω_{NL}/ω_L of the auxetic laminated plate with magneto-electro-elastic face sheets with $a/b = 1,\ h = 0.05\,m,\ h_c/h_f = 8,\ b/h = 20,\ t/l = 0.0138571,\ \theta = 30^0,\ d/l = 2$.

$\psi_0\,(A)$	$\phi_0\,(V)$	ξ/h				
		0.2	0.4	0.6	0.8	1
−200	−400	1.003664	1.014576	1.032507	1.057100	1.087902
	0	1.003665	1.014582	1.032520	1.057121	1.087935
	400	1.003667	1.014588	1.032532	1.057143	1.087968
0	−400	1.003649	1.014519	1.032381	1.056880	1.087569
	0	1.003651	1.014525	1.032393	1.056902	1.087602
	400	1.003652	1.014530	1.032406	1.056924	1.087635
200	−400	1.003635	1.014462	1.032255	1.056662	1.087238
	0	1.003637	1.014468	1.032268	1.056684	1.087271
	400	1.003638	1.014474	1.03228	1.056705	1.087303

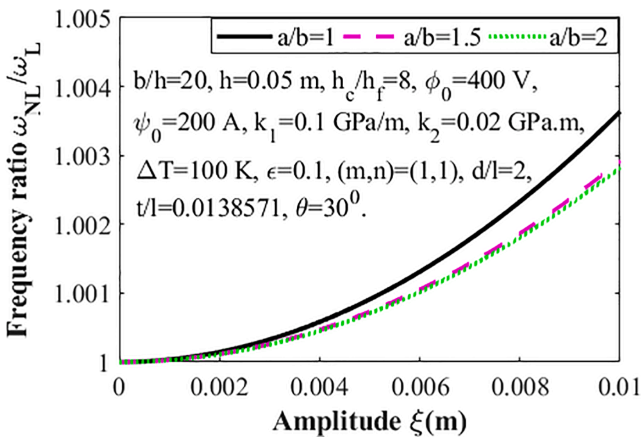

Fig. 3. Effects of the plate length to width ratio a/b on the nonlinear to linear frequency ratio – dimensionless amplitude curves of the auxetic laminated plate with magneto-electro-elastic face sheets.

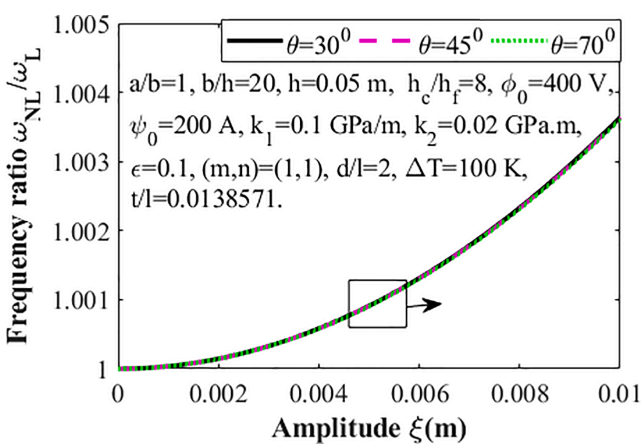

Fig. 4. Effects of the inclined angle of unit cells θ on the nonlinear to linear frequency ratio – dimensionless amplitude curves of the auxetic laminated plate with magneto-electro-elastic face sheets.

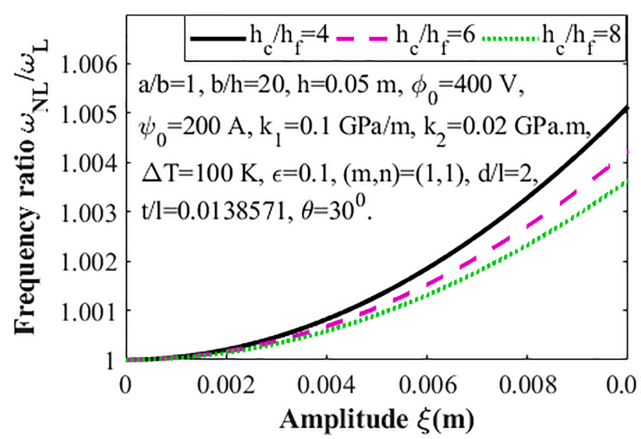

Fig. 5. Effects of the core thickness to face sheet thickness ratio h_c/h_f on the nonlinear to linear frequency ratio – dimensionless amplitude curves of the auxetic laminated plate with magneto-electro-elastic face sheets.

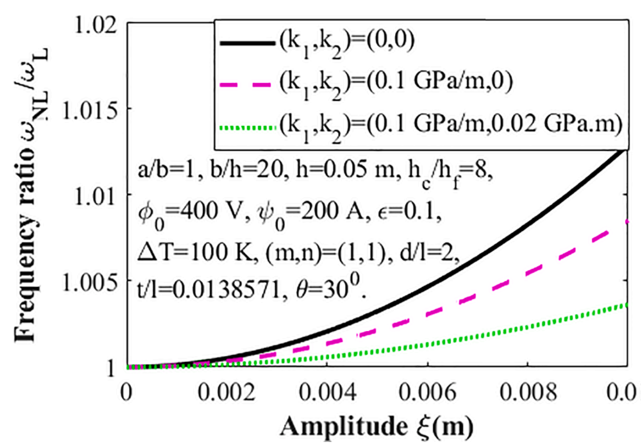

Fig. 6. Effects of two elastic foundations coefficients on the nonlinear to linear frequency ratio – dimensionless amplitude curves of the auxetic laminated plate with magneto-electro-elastic face sheets.

elastic modulus of the auxetic laminated plate decreases when the temperature increment is increased. The results from Table 8 also show that the increase of ratio b/h yields the reduction of the frequency ratio.

The influences of magnetic and electric potentials ψ_0 and ϕ_0 on the nonlinear to linear frequency ratio ω_{NL}/ω_L of the auxetic laminated plate with magneto-electro-elastic face sheets are shown in Table 9. Two elastic foundations coefficients are $k_1 = 0.1\,GPa/m,\ k_2 = 0.02\,GPa.m$ and the temperature increment is $\Delta T = 100\,K$. Obviously, the frequency ratio becomes higher when the magnetic potential decreases and change into lower when the electric potential decreases although the differences are small.

The effects of the plate length to width ratio a/b on the nonlinear to linear frequency ratio – dimensionless amplitude curves of the auxetic laminated plate with magneto-electro-elastic face sheets is indicated in Fig. 3. The electric and magnetic potentials are chosen to be $\phi_0 = 400\ V$, $\psi_0 = 200\,A$. As can be seen, the ratio a/b affect significantly on the frequency ratio of the auxetic laminated plate; the higher the ratio a/b is, the lower frequency ratio is.

Fig. 4 shows the effect of the inclined angle θ of unit cells on the nonlinear to linear frequency ratio – dimensionless amplitude curves of

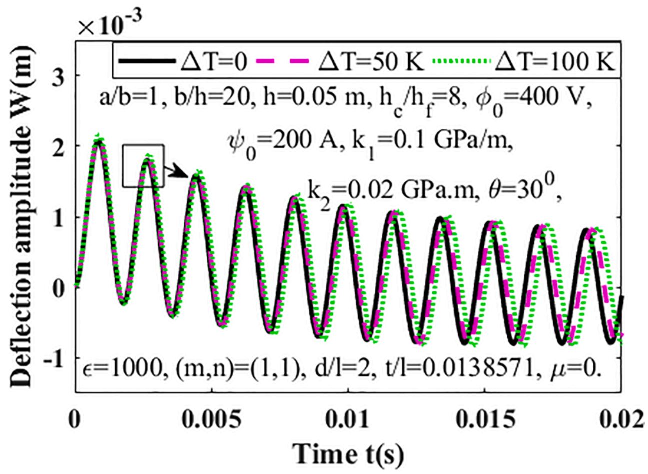

Fig. 7. Effects of temperature increment ΔT on the nonlinear dynamic response of the auxetic laminated plate with magneto-electro-elastic face sheets.

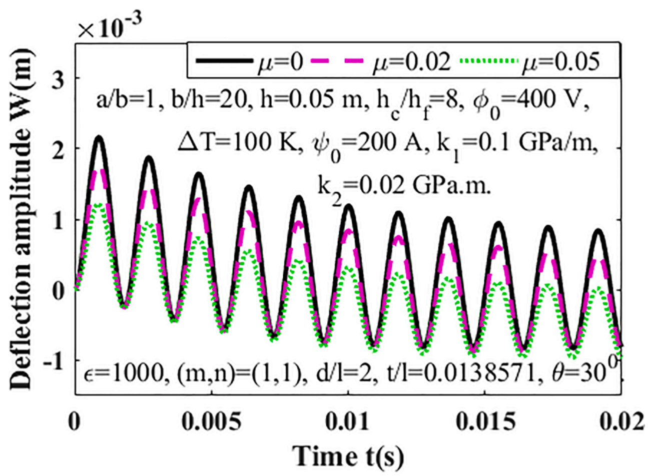

Fig. 8. Effects of initial imperfection parameter on the nonlinear dynamic response of the auxetic laminated plate with magneto-electro-elastic face sheets.

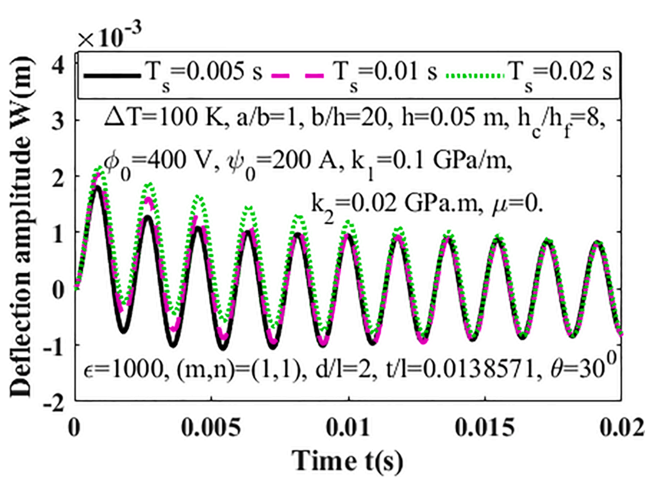

Fig. 9. Effects of parameter of blast loading on the nonlinear dynamic response of the auxetic laminated plate with magneto-electro-elastic face sheets.

the auxetic laminated plate with magneto-electro-elastic face sheets. As can be observed, the effect of the inclined angle is extremely weak, which can only be seen clearly by zooming in on the obtained figure. The frequency ratio of the auxetic laminated plate decreases when the inclined angle increases. It is reasonable conclusion because the rise of the inclined angle results in the increase of the structural stiffness of core layer.

Fig. 5 presents the effect of the core thickness to face sheet thickness ratio h_c/h_f on the relationship between the nonlinear to linear frequency ratio and dimensionless amplitude curves of the auxetic laminated plate with magneto-electro-elastic face sheets. Three values of ratio $h_c/h_f = 4,\ 6,\ 8$ are used in this figure. The geometrical parameters of unit cells are taken to be $d/l = 2,\ t/l = 0.0138571,\ \theta = 30^0$. It can be found that the frequency ratio becomes higher as the ratio h_c/h_f decreases. This is due to the reduction of structural stiffness by decrease the ratio between the core thickness and the face sheet thickness.

Fig. 6 indicates the effect of two elastic foundations coefficients $k_1\ (GPa/m)$ and $k_2\ (GPa.m)$ on the nonlinear to linear frequency ratio – dimensionless amplitude curves of the auxetic laminated plate with magneto-electro-elastic face sheets. The geometrical and material parameters are chosen to be $a/b = 1,\ b/h = 20,\ h_c/h_f = 8,\ d/l = 2,\ \theta = 30^0$. The results from Fig. 6 show that the frequency ratio decreases considerably when two coefficients k_1 and k_2 increase. The reason for this trend is that the structural stiffness and elastic modulus of the auxetic laminated plate increase with increasing two elastic foundations coefficients. Besides, it is easy to see that the effect of Pasternak foundation with shear layer stiffness k_2 is greater than one of Winkler foundation with modulus k_1 .

Fig. 7 shows the effects of temperature increment $\Delta T\,(K)$ on the nonlinear dynamic response of the auxetic laminated plate with magneto-electro-elastic face sheets subjected to thermal, mechanical and electrical loadings. The electric and magnetic potentials are taken to be $\phi_0 = 400\ V,\ \psi_0 = 200\,A$. As can be seen, the value of deflection amplitude decreases to 0 when the time increases due to the impact of blast loading. Besides, it is found here that the temperature increment has weak effect on the deflection amplitude – time curves of the auxetic laminated plate. The deflection amplitude increases slightly when the temperature increment is increased. The possible reason is that the structural stiffness and elastic modulus of the auxetic laminated plate decreases with increasing temperature increment.

Fig. 8 indicates the effect of initial imperfection parameter on the nonlinear dynamic response of the auxetic laminated plate with magneto-electro-elastic face sheets subjected to thermal, mechanical and electrical loadings. Three values of $\mu = 0,\ 0.01$ and 0.02 are considered. It is found that the positive value of deflection amplitude decreases significantly when the initial imperfection parameter increases. However, the increase of the initial imperfection parameter results in the rise of the negative value of deflection amplitude.

Fig. 9 presents the nonlinear dynamic response of the auxetic laminated plate with magneto-electro-elastic face sheets with different values of parameter of blast loading T_s . The geometrical parameters are taken to be $a/b = 1,\ b/h = 20,\ h_c/h_f = 8$ and the temperature increment is chosen as $\Delta T = 100\,K$. Obviously, the deflection amplitude is increased with increasing of the parameter T_s of blast loading. The reason is that the value of blast loading is increased when the value of parameter T_s increases.

5. Conclusions

Based on the Reddy's higher order shear deformation plate theory, the nonlinear vibration of the auxetic laminated plate with magneto-electro-elastic face sheets subjected to the combination of blast, thermal, electric and magnetic loadings is presented. The natural frequency, the relationship between frequency ratio and dimensionless amplitude and the dynamic response of the auxetic laminated plate are obtained by using Galerkin and Runge-Kutta methods. From numerical results, several conclusions are obtained as follows

(1) The natural frequency is increased and the frequency ratio is decreased with increasing two elastic foundations coefficients.
(2) The increase of temperature increment, electric potential and the decrease of magnetic potential result in the decrease of natural frequency and the increase of frequency ratio.
(3) The effect of the inclined angle of unit cells of auxetic core layer is considerable. As the inclined angle increases, both of the natural frequency and the frequency ratio decreases.
(4) As the initial imperfection parameter is increased, the deflection amplitude decreases significantly.
(5) The geometrical parameters have strong influences on the vibration characteristics of the auxetic laminated plate.

Funding

This research is funded by Vietnam National Foundation for Science and Technology Development (NAFOSTED) under grant number 107.02-2019.01. The authors are grateful for this support.

Declaration of Competing Interest

The authors declare that they have no known competing financial interests or personal relationships that could have appeared to influence the work reported in this paper.

Appendix A

$$\overline{C_{11}} = C_{11}^f - \frac{(C_{13}^f)^2}{C_{33}^f},\ \overline{C_{12}} = C_{12}^f - \frac{C_{13}^f C_{23}^f}{C_{33}^f},\ \overline{C_{22}} = C_{22}^f - \frac{(C_{23}^f)^2}{C_{33}^f},\ \overline{C_{44}} = C_{44}^f,\ \overline{C_{55}} = C_{55}^f,$$

$$\overline{C_{66}} = C_{66}^f,\ \overline{e_{31}} = e_{31}^f - \frac{C_{13}^f e_{33}^f}{C_{33}^f},\ \overline{e_{32}} = e_{32}^f - \frac{C_{23}^f e_{33}^f}{C_{33}^f},\ \overline{e_{15}} = e_{15}^f,\ \overline{e_{24}} = e_{24}^f,\ \overline{q_{31}} = q_{31}^f - \frac{C_{13}^f q_{33}^f}{C_{33}^f},$$

$$\overline{q_{32}} = q_{32}^f - \frac{C_{23}^f q_{33}^f}{C_{33}^f},\ \overline{q_{15}} = q_{15}^f,\ \overline{q_{24}} = q_{24}^f,\ \overline{\mu_{11}} = \mu_{11}^f,\ \overline{\mu_{22}} = \mu_{22}^f,\ \overline{\mu_{33}} = \mu_{33}^f + \frac{(q_{33}^f)^2}{C_{33}^f},$$

$$\overline{\eta_{11}} = \eta_{11}^f,\ \overline{\eta_{22}} = \eta_{22}^f,\ \overline{\eta_{33}} = \eta_{33}^f + \frac{(e_{33}^f)^2}{C_{33}^f},\ \overline{m_{11}} = m_{11}^f,\ \overline{m_{22}} = m_{22}^f,\ \overline{m_{33}} = m_{33}^f + \frac{e_{33}^f q_{33}^f}{C_{33}^f},$$

$$\overline{\alpha_1} = \alpha_1^f - \frac{C_{13}^f \alpha_3^f}{C_{33}^f},\ \overline{\alpha_2} = \alpha_2^f - \frac{C_{23}^f \alpha_3^f}{C_{33}^f},\ \overline{p_1} = p_1^f,\ \overline{p_2} = p_2^f,\ \overline{p_3} = p_3^f + \frac{e_{33}^f \alpha_{33}^f}{C_{33}^f},$$

$$\overline{\lambda_1} = \lambda_1^f,\ \overline{\lambda_2} = \lambda_2^f,\ \overline{\lambda_3} = \lambda_3^f + \frac{q_{33}^f \alpha_{33}^f}{C_{33}^f}.$$

Appendix B

$$(A_{ij},\ B_{ij},\ D_{ij},\ E_{ij},\ F_{ij},\ H_{ij}) = \int_{-h_f - h_c/2}^{-h_c/2} \overline{C_{ij}}(1,\ z,\ z^2,\ z^3,\ z^4,\ z^6)\,dz + \int_{-h_c/2}^{h_c/2} Q_{ij}^c(1,\ z,\ z^2,\ z^3,\ z^4,\ z^6)\,dz$$

$$+ \int_{h_c/2}^{h_c/2 + h_f} \overline{C_{ij}}(1,\ z,\ z^2,\ z^3,\ z^4,\ z^6)\,dz,\ ij = 11, 12, 22, 66,$$

$$(A_{kl},\ D_{kl},\ F_{kl}) = \int_{-h_f - h_c/2}^{-h_c/2} \overline{C_{ij}}(1,\ z^2,\ z^4)\,dz + \int_{-h_c/2}^{h_c/2} Q_{ij}^c(1,\ z^2,\ z^4)\,dz$$

$$+ \int_{h_c/2}^{h_c/2 + h_f} \overline{C_{ij}}(1,\ z^2,\ z^4)\,dz,\ kl = 44, 55,\ \ \Phi_i = \int_{-h_f - h_c/2}^{-h_c/2} \overline{e_{31}}\,(1, z, z^3)dz + \int_{h_c/2}^{h_f + h_c/2} \overline{e_{31}}\,(1, z, z^3)dz,$$

$$\Gamma_i = \int_{-h_f - h_c/2}^{-h_c/2} \overline{q_{31}}\,(1, z, z^3)\,dz + \int_{h_c/2}^{h_f + h_c/2} \overline{q_{31}}\,(1, z, z^3)dz,\ i = 1, 3, 5$$

$$\Phi_j = \int_{-h_f - h_c/2}^{-h_c/2} \overline{e_{32}}\,(1, z, z^3)\,dz + \int_{h_c/2}^{h_f + h_c/2} \overline{e_{32}}\,(1, z, z^3)dz,\ j = 2, 4, 6,$$

$$\Gamma_j = \int_{-h_f - h_c/2}^{-h_c/2} \overline{q_{32}}\,(1, z, z^3)\,dz + \int_{h_c/2}^{h_f + h_c/2} \overline{q_{32}}\,(1, z, z^3)\,dz,\ j = 2, 4, 6,$$

$$\alpha_i = \int_{-h_f - h_c/2}^{-h_c/2} (\overline{C_{11}} + \overline{C_{12}})\overline{\alpha_1}\,(1, z, z^3)\,dz + \int_{-h_c/2}^{h_c/2} Q_{11}^c \alpha_{11}^c\,(1, z, z^3)dz$$

$$+ \int_{-h_c/2}^{h_c/2} Q_{12}^c \alpha_{22}^c\,(1, z, z^3)\,dz + \int_{h_c/2}^{h_f + h_c/2} (\overline{C_{11}} + \overline{C_{12}})\overline{\alpha_1}\,(1, z, z^3)\,dz,\ i = 1, 3, 5,$$

$$\alpha_j = \int_{-h_f - h_c/2}^{-h_c/2} (\overline{C_{12}} + \overline{C_{22}})\overline{\alpha_2}\,(1, z, z^3)\,dz + \int_{-h_c/2}^{h_c/2} Q_{12}^c \alpha_{11}^c\,(1, z, z^3)dz$$

$$+\int_{-h_c/2}^{h_c/2} Q_{22}^{c}\alpha_{22}^{c}\left(1,z,z^3\right)dz+\int_{h_c/2}^{h_f+h_c/2}(\overline{C_{12}}+\overline{C_{22}})\overline{\alpha_2}\left(1,z,z^3\right)dz,\ j=2,4,6,$$

$$\Phi_k=\int_{-h_f-h_c/2}^{-h_c/2}\overline{e_{24}}\left(1,z^2\right)dz+\int_{h_c/2}^{h_f+h_c/2}\overline{e_{24}}\left(1,z^2\right)dz,\ k=8,10,$$

$$\Gamma_k=\int_{-h_f-h_c/2}^{-h_c/2}\overline{q_{24}}\left(1,z^2\right)dz+\int_{h_c/2}^{h_f+h_c/2}\overline{q_{24}}\left(1,z^2\right)dz,k=8,10,$$

$$\Phi_k=\int_{-h_f-h_c/2}^{-h_c/2}\overline{e_{15}}\left(1,z^2\right)dz+\int_{h_c/2}^{h_f+h_c/2}\overline{e_{15}}\left(1,z^2\right)dz,k=8,10,$$

$$\Gamma_l=\int_{-h_f-h_c/2}^{-h_c/2}\overline{q_{15}}\left(1,z^2\right)dz+\int_{h_c/2}^{h_f+h_c/2}\overline{q_{15}}\left(1,z^2\right)dz,l=7,9.$$

Appendix C

$$L_{11}(w)=Y_{11}\frac{\partial^2 w}{\partial x^2}+Y_{12}\frac{\partial^2 w}{\partial y^2}+Y_{13}\frac{\partial^4 w}{\partial x^4}+Y_{14}\frac{\partial^4 w}{\partial x^2\partial y^2}+Y_{15}\frac{\partial^4 w}{\partial y^4}-k_1 w+k_2\left(\frac{\partial^2 w}{\partial x^2}+\frac{\partial^2 w}{\partial y^2}\right),$$

$$L_{12}(\phi_x)=Y_{11}\frac{\partial\phi_x}{\partial x}+Y_{16}\frac{\partial^3\phi_x}{\partial x^3}+Y_{17}\frac{\partial^3\phi_x}{\partial x\partial y^2},\ L_{13}\left(\phi_y\right)=Y_{12}\frac{\partial\phi_y}{\partial y}+Y_{18}\frac{\partial^3\phi_y}{\partial y^3}+Y_{19}\frac{\partial^3\phi_y}{\partial x^2\partial y},$$

$$L_{14}(f)=Y_{110}\frac{\partial^4 f}{\partial x^4}+Y_{111}\frac{\partial^4 f}{\partial x^2\partial y^2}+Y_{112}\frac{\partial^4 f}{\partial y^4},$$

$$L_{15}(\Phi)=(Y_{114}cos(\beta z)-Y_{115}\beta sin(\beta z))\frac{\partial^2\Phi}{\partial^2 x}+(Y_{113}cos(\beta z)-Y_{116}\beta sin(\beta z))\frac{\partial^2\Phi}{\partial^2 y},$$

$$L_{16}(\Psi)=(Y_{118}cos(\beta z)-Y_{119}\beta sin(\beta z))\frac{\partial^2\Psi}{\partial^2 x}+(Y_{117}cos(\beta z)-Y_{120}\beta sin(\beta z))\frac{\partial^2\Psi}{\partial^2 y},$$

$$S(w,f)=\frac{\partial^2 f}{\partial y^2}\frac{\partial^2 w}{\partial x^2}-2\frac{\partial^2 f}{\partial x\partial y}\frac{\partial^2 w}{\partial y^2}+\frac{\partial^2 f}{\partial x^2}\frac{\partial^2 w}{\partial y^2},$$

$$L_{21}(w)=Y_{21}\frac{\partial w}{\partial x}+Y_{22}\frac{\partial^3 w}{\partial x^3}+Y_{23}\frac{\partial^3 w}{\partial x\partial y^2},\ L_{22}(\phi_x)=Y_{21}\phi_x+Y_{24}\frac{\partial^2\phi_x}{\partial x^2}+Y_{25}\frac{\partial^2\phi_x}{\partial y^2},$$

$$L_{23}\left(\phi_y\right)=Y_{26}\frac{\partial^2\phi_y}{\partial x\partial y},\ L_{24}(f)=Y_{27}\frac{\partial^3 f}{\partial x^3}+Y_{28}\frac{\partial^3 f}{\partial x\partial y^2},$$

$$L_{25}(\Phi)=-(Y_{114}cos(\beta z)+Y_{29}\beta sin(\beta z))\frac{\partial\Phi}{\partial x},$$

$$L_{26}(\Psi)=-(Y_{118}cos(\beta z)+Y_{210}\beta sin(\beta z))\frac{\partial\Psi}{\partial x},$$

$$L_{31}(w)=Y_{31}\frac{\partial w}{\partial y}+Y_{32}\frac{\partial^3 w}{\partial x^2\partial y}+Y_{33}\frac{\partial^3 w}{\partial y^3},\ \ L_{32}(\phi_x)=Y_{34}\frac{\partial^2\phi_x}{\partial x\partial y},$$

$$L_{33}\left(\phi_y\right)=Y_{31}\phi_y+Y_{35}\frac{\partial^2\phi_y}{\partial x^2}+Y_{36}\frac{\partial^2\phi_y}{\partial y^2},\ L_{34}(f)=Y_{37}\frac{\partial^3 f}{\partial x^2\partial y}+Y_{38}\frac{\partial^3 f}{\partial y^3},$$

$$L_{35}(\Phi)=-(Y_{113}cos(\beta z)+Y_{39}\beta sin(\beta z))\frac{\partial\Phi}{\partial y},$$

$$L_{36}(\Psi)=-(Y_{117}cos(\beta z)+Y_{310}\beta sin(\beta z))\frac{\partial\Psi}{\partial y},$$

$$Y_{111}=-c_1(2E_{66}I_{31}-E_{11}I_{11}+2E_{12}I_{12}-E_{22}I_{21}),\ Y_{112}=c_1(E_{12}I_{11}-E_{22}I_{12}),$$

$$Y_{113}=\Phi_8-3c_1\Phi_{10},Y_{114}=\Phi_7-3c_1\Phi_9,Y_{115}=-c_1\Phi_5,Y_{116}=-c_1\Phi_6,$$

$$Y_{117}=\Gamma_8-3c_1\Gamma_{10},Y_{118}=\Gamma_7-3c_1\Gamma_9,Y_{119}=-c_1\Gamma_5,Y_{120}=-c_1\Gamma_6,$$

$$
\begin{gathered}
Y_{21} = -A_{44} + 6c_1D_{44} - 9c_1^2F_{44},\ Y_{22} = -c_1(F_{11} + B_{11}I_{15} + B_{12}I_{25} - c_1E_{11}I_{15} - c_1H_{11} - c_1E_{12}I_{25}),\\
Y_{23} = -c_1(B_{11}I_{16} + B_{12}I_{26} + F_{12} + 2B_{66}I_{33} + 2F_{66} - 2c_1E_{66}I_{33} - 2c_1H_{66} - c_1E_{12}I_{26} - c_1E_{11}I_{16} - c_1H_{12}),\\
Y_{24} = B_{11}I_{13} - c_1B_{11}I_{15} + D_{11} - c_1F_{11} + B_{12}I_{23} - c_1B_{12}I_{25} - c_1E_{11}I_{13} + c_1^2E_{11}I_{15} - c_1F_{11} + c_1^2H_{11}\\
-c_1E_{12}I_{23} + c_1^2E_{12}I_{25},\ Y_{25} = B_{66}I_{32} - c_1B_{66}I_{33} + D_{66} - c_1F_{66} - c_1E_{66}I_{32} + c_1^2E_{66}I_{33} - c_1F_{66} + c_1^2H_{66},\\
Y_{26} = B_{11}I_{14} - c_1B_{11}I_{16} + B_{12}I_{24} - c_1B_{12}I_{26} + D_{12} - c_1F_{12} + B_{66}I_{32} - c_1B_{66}I_{33} + D_{66} - c_1F_{66} - c_1E_{66}I_{32}\\
+c_1^2E_{66}I_{33} - c_1F_{66} + c_1^2H_{66} - c_1E_{11}I_{14} + c_1^2E_{11}I_{16} - c_1E_{12}I_{24} - c_1F_{12} + c_1^2E_{12}I_{26} + c_1^2H_{12},\\
Y_{27} = -B_{11}I_{12} + B_{12}I_{21} + c_1E_{11}I_{12} - c_1E_{12}I_{21},\ Y_{28} = B_{11}I_{11} - B_{66}I_{31} - B_{12}I_{12} - c_1E_{11}I_{11} + c_1E_{12}I_{12}\\
+c_1E_{66}I_{31}, Y_{29} = -\Phi_3 + c_1\Phi_5, Y_{210} = -\Gamma_3 + c_1\Gamma_5, Y_{31} = -A_{55} + 6c_1D_{55} - 9c_1^2F_{55},\\
Y_{32} = -c_1(2B_{66}I_{33} + 2F_{66} + B_{12}I_{15} + F_{12} + B_{22}I_{25} - 2c_1E_{66}I_{33} - 2c_1H_{66} - c_1H_{12} - c_1E_{12}I_{15} - c_1E_{22}I_{25}),\\
Y_{33} = -c_1(B_{12}I_{16} + B_{22}I_{26} + F_{22} - c_1E_{12}I_{16} - c_1E_{22}I_{26} - c_1H_{22}),\\
Y_{34} = B_{66}I_{32} - c_1B_{66}I_{33} + D_{66} - c_1F_{66} + B_{12}I_{13} - c_1B_{12}I_{15} + D_{12} - c_1F_{12} + B_{22}I_{23} - c_1B_{22}I_{25} - c_1E_{66}I_{32}\\
+c_1^2E_{66}I_{33} - c_1F_{66} + c_1^2H_{66} - c_1E_{12}I_{13} + c_1^2E_{12}I_{15} - c_1F_{12} + c_1^2H_{12} - c_1E_{22}I_{23} + c_1^2E_{22}I_{25},\\
Y_{35} = B_{66}I_{32} - c_1B_{66}I_{33} + D_{66} - c_1F_{66} - c_1E_{66}I_{32} + c_1^2E_{66}I_{33} - c_1F_{66} + c_1^2H_{66},\\
Y_{36} = B_{12}I_{14} - c_1B_{12}I_{16} + B_{22}I_{24} - c_1B_{22}I_{26} + D_{22} - c_1F_{22} - c_1E_{12}I_{14} + c_1^2E_{12}I_{16} - c_1E_{22}I_{24}\\
+c_1^2E_{22}I_{26} - c_1F_{22} + c_1^2H_{22},\ Y_{37} = -B_{12}I_{12} - B_{66}I_{31} + B_{22}I_{21} + c_1E_{66}I_{31} + c_1E_{12}I_{12} - c_1E_{22}I_{21},\\
Y_{38} = B_{12}I_{11} - B_{22}I_{12} - c_1E_{12}I_{11} + c_1E_{22}I_{12}, Y_{39} = -\Phi_4 + c_1\Phi_6, X_{310} = -\Gamma_4 + c_1\Gamma_6.
\end{gathered}
$$

Appendix D

$$
\begin{gathered}
l_{11} = -k_1 - k_2\left(\lambda_m^2 + \delta_n^2\right) + Y_{13}\lambda_m^4 + Y_{14}\lambda_m^2\delta_n^2 + Y_{15}\delta_n^4 + Y_{110}Q_1\lambda_m^4 + Y_{111}Q_1\lambda_m^2\delta_n^2 + Y_{112}Q_1\delta_n^4,\\
l_{12} = -Y_{11}\lambda_m + Y_{16}\lambda_m^3 + Y_{17}\lambda_m\delta_n^2 + Y_{110}Q_2\lambda_m^4 + Y_{111}Q_2\lambda_m^2\delta_n^2 + Y_{112}Q_2\delta_n^4,\\
l_{13} = -Y_{12}\delta_n + Y_{18}\delta_n^3 + Y_{19}\lambda_m^2\delta_n + Y_{110}Q_3\lambda_m^4 + Y_{111}Q_3\lambda_m^2\delta_n^2 + Y_{112}Q_3\delta_n^4,\\
l_{14} = \frac{32Q_2\lambda_m\delta_n}{3ab},\ l_{15} = \frac{32Q_3\lambda_m\delta_n}{3ab},\ l_{16} = \beta sin(\beta z)\left(\lambda_m^2Y_{115} + \delta_n^2Y_{116}\right),\\
l_{17} = \beta sin(\beta z)\left(Y_{119}\lambda_m^2 + Y_{120}\delta_n^2\right), n_1 = -Y_{11}\lambda_m^2 - Y_{12}\delta_n^2,\ n_2 = \frac{32Q_1\lambda_m\delta_n}{3ab},\\
n_3 = -\frac{8Y_{110}\lambda_m\delta_n}{3abI_{21}} - \frac{8Y_{112}\lambda_m\delta_n}{3abI_{11}},\ n_4 = -\frac{\lambda_m^4}{16I_{11}} - \frac{\delta_n^4}{16I_{21}},\ n_5 = \frac{16}{mn\pi^2},\\
l_{21} = -\lambda_m^3(Y_{22} + Q_1Y_{27}) - \lambda_m\delta_n^2(Y_{23} + Q_1Y_{28}),\\
l_{22} = Y_{21} - Y_{24}\lambda_m^2 - Y_{25}\delta_n^2 - Y_{27}Q_2\lambda_m^3 - Y_{28}Q_2\lambda_m\delta_n^2,\\
l_{23} = -Y_{26}\lambda_m\delta_n - Y_{27}Q_3\lambda_m^3 - Y_{28}Q_3\lambda_m\delta_n^2,\ l_{24} = -Y_{29}\beta sin(\beta z)\lambda_m,\\
l_{25} = -Y_{210}\beta sin(\beta z)\lambda_m,\ n_6 = Y_{21}\lambda_m,\ n_7 = \frac{8Y_{27}\delta_n}{3abI_{21}},\ l_{31} = -\delta_n^3(Y_{33} + Q_1Y_{38})\\
-\lambda_m^2\delta_n(Y_{32} + Q_1Y_{37}),\ l_{32} = -Y_{34}\lambda_m\delta_n - Y_{38}Q_2\delta_n^3 - D_{37}Q_2\lambda_m^2\delta_n,\ l_{33} = Y_{31} - Y_{35}\lambda_m^2 - Y_{36}\delta_n^2\\
-Y_{38}Q_3\delta_n^3 - Y_{37}Q_3\lambda_m^2\delta_n, l_{34} = -Y_{39}\beta sin(\beta z)\delta_n,\\
l_{35} = -Y_{310}\beta sin(\beta z)\delta_n,\ n_8 = Y_{31}\delta_n,\ n_9 = \frac{8Y_{38}\lambda_m}{3abI_{11}},\\
l_{41} = -\left(O_{11}\lambda_m^2 + O_{12}\delta_n^2\right) + \left(c_1(O_{14})\lambda_m^2 + c_1(O_{16})\delta_n^2\right)\\
l_{42} = -(O_{11} + O_{13} - c_1O_{14})\lambda_m, l_{43} = -(O_{12} + O_{15} - c_1O_{16})\delta_n,\\
l_{44} = \left(-\lambda_m^2\eta_{11}^* - \delta_n^2\eta_{22}^*\right)cos(\beta z) - \beta sin(\beta z)\eta_{33}^*,\\
l_{45} = \left(-\lambda_m^2m_{11}^* - \delta_n^2m_{22}^*\right)cos(\beta z) - \beta sin(\beta z)m_{33}^*,\\
l_{51} = -\left(O_{21}\lambda_m^2 + O_{22}\delta_n^2\right) + \left(c_1(O_{24})\lambda_m^2 + c_1(O_{26})\delta_n^2\right)\\
l_{52} = -(O_{21} + O_{23} - c_1O_{24})\lambda_m,\\
l_{53} = -(O_{22} + O_{25} - c_1O_{26})\delta_n,\\
l_{54} = \left(-\lambda_m^2m_{11}^* - \delta_n^2m_{22}^*\right)cos(\beta z) - \beta sin(\beta z)m_{33}^*,\\
l_{55} = \left(-\lambda_m^2\mu_{11}^* - \delta_n^2\mu_{22}^*\right)cos(\beta z) - \beta sin(\beta z)\mu_{33}^*,
\end{gathered}
$$

$$O_{11}=\int_{-h_f-h_c/2}^{h_c/2}e_{15}\left(1-3c_1z^2\right)\cos(\beta z)dz+\int_{-h_c/2}^{h_c/2+h_f}e_{15}\left(1-3c_1z^2\right)\cos(\beta z)dz,$$
$$\eta_{11}^{*}=\int_{-h_f-h_c/2}^{h_c/2}e_{15}\eta_{11}\cos(\beta z)dz+\int_{-h_c/2}^{h_c/2+h_f}e_{15}\eta_{11}\cos(\beta z)dz,$$
$$m_{11}^{*}=\int_{-h_f-h_c/2}^{h_c/2}m_{11}\cos(\beta z)dz+\int_{-h_c/2}^{h_c/2+h_f}m_{11}\cos(\beta z)dz,$$
$$O_{12}=\int_{-h_f-h_c/2}^{h_c/2}e_{24}\left(1-3c_1z^2\right)\cos(\beta z)dz+\int_{-h_c/2}^{h_c/2+h_f}e_{24}\left(1-3c_1z^2\right)\cos(\beta z)dz,$$
$$\eta_{22}^{*}=\int_{-h_f-h_c/2}^{h_c/2}\eta_{22}\cos(\beta z)dz+\int_{-h_c/2}^{h_c/2+h_f}\eta_{22}\cos(\beta z)dz,$$
$$m_{22}^{*}=\int_{-h_f-h_c/2}^{h_c/2}m_{22}\cos(\beta z)dz+\int_{-h_c/2}^{h_c/2+h_f}m_{22}\cos(\beta z)dz,$$

$$(O_{13},O_{14})=\int_{-h_f-h_c/2}^{h_c/2}e_{31}\left(z,z^3\right)\beta\sin(\beta z)dz+\int_{-h_c/2}^{h_c/2+h_f}e_{31}\left(z,z^3\right)\beta\sin(\beta z)dz,$$
$$\eta_{33}^{*}=\int_{-h_f-h_c/2}^{h_c/2}\eta_{33}\beta\sin(\beta z)dz+\int_{-h_c/2}^{h_c/2+h_f}\eta_{33}\beta\sin(\beta z)dz,$$
$$m_{33}^{*}=\int_{-h_f-h_c/2}^{h_c/2}m_{33}\beta\sin(\beta z)dz+\int_{-h_c/2}^{h_c/2+h_f}m_{33}\beta\sin(\beta z)dz,$$

$$(O_{15},O_{16})=\int_{-h_f-h_c/2}^{h_c/2}e_{32}\left(z,z^3\right)\beta\sin(\beta z)dz+\int_{-h_c/2}^{h_c/2+h_f}e_{32}\left(z,z^3\right)\beta\sin(\beta z)dz,$$
$$O_{21}=\int_{-h_f-h_c/2}^{h_c/2}q_{15}\left(1-3c_1z^2\right)\cos(\beta z)dz+\int_{-h_c/2}^{h_c/2+h_f}q_{15}\left(1-3c_1z^2\right)\cos(\beta z)dz,$$
$$m_{11}^{*}=\int_{-h_f-h_c/2}^{h_c/2}m_{11}\cos(\beta z)dz+\int_{-h_c/2}^{h_c/2+h_f}m_{11}\cos(\beta z)dz,$$
$$\mu_{11}^{*}=\int_{-h_f-h_c/2}^{h_c/2}\mu_{11}\cos(\beta z)dz+\int_{-h_c/2}^{h_c/2+h_f}\mu_{11}\cos(\beta z)dz,$$

$$O_{22}=\int_{-h_f-h_c/2}^{h_c/2}q_{24}\left(1-3c_1z^2\right)\cos(\beta z)dz+\int_{-h_c/2}^{h_c/2+h_f}q_{24}\left(1-3c_1z^2\right)\cos(\beta z)dz,$$
$$m_{22}^{*}=\int_{-h_f-h_c/2}^{h_c/2}m_{22}\cos(\beta z)dz+\int_{-h_c/2}^{h_c/2+h_f}m_{22}\cos(\beta z)dz,$$
$$\mu_{22}^{*}=\int_{-h_f-h_c/2}^{h_c/2}\mu_{22}\cos(\beta z)dz+\int_{-h_c/2}^{h_c/2+h_f}\mu_{22}\cos(\beta z)dz,$$

$$(O_{23},O_{24})=\int_{-h_f-h_c/2}^{h_c/2}q_{31}\left(z,z^3\right)\beta\sin(\beta z)dz+\int_{-h_c/2}^{h_c/2+h_f}q_{31}\left(z,z^3\right)\beta\sin(\beta z)dz,$$
$$(O_{25},O_{26})=\int_{-h_f-h_c/2}^{h_c/2}q_{32}\left(z,z^3\right)\beta\sin(\beta z)dz+\int_{-h_c/2}^{h_c/2+h_f}q_{32}\left(z,z^3\right)\beta\sin(\beta z)dz.$$

Appendix E

$$g_1=\frac{(I_{21}a_1+I_{12}a_4)}{ab\left(I_{12}^2-I_{11}I_{21}\right)}\frac{4}{\lambda_m\delta_n},g_4=-\frac{1}{8}\frac{\left(I_{21}\lambda_m^2+I_{12}\delta_n^2\right)}{\left(I_{12}^2-I_{11}I_{21}\right)},$$
$$g_2=\frac{(I_{21}a_2+I_{12}a_5)}{ab\left(I_{12}^2-I_{11}I_{21}\right)}\frac{4}{\lambda_m\delta_n},g_3=\frac{(I_{21}a_3+I_{12}a_6)}{ab\left(I_{12}^2-I_{11}I_{21}\right)}\frac{4}{\lambda_m\delta_n},$$
$$g_5=\frac{(I_{17}I_{21}+I_{27}I_{12})}{\left(I_{12}^2-I_{11}I_{21}\right)},g_6=\frac{(I_{18}I_{21}+I_{28}I_{12})}{\left(I_{12}^2-I_{11}I_{21}\right)},g_7=\frac{(I_{19}I_{21}+I_{29}I_{12})}{\left(I_{12}^2-I_{11}I_{21}\right)},$$

$$f_1 = \frac{(a_1 I_{12} + I_{11} a_4)}{ab\left(I_{12}^2 - I_{11} I_{21}\right)} \frac{4}{\lambda_m \delta_n}, f_4 = -\frac{1}{8} \frac{\left(\lambda_m^2 I_{12} + I_{11} \delta_{12}^2\right)}{\left(I_{12}^2 - I_{11} I_{21}\right)},$$

$$f_2 = \frac{(a_2 I_{12} + I_{11} a_5)}{ab\left(I_{12}^2 - I_{11} I_{21}\right)} \frac{4}{\lambda_m \delta_n}, f_3 = \frac{(a_3 I_{12} + I_{11} a_6)}{ab\left(I_{12}^2 - I_{11} I_{21}\right)} \frac{4}{\lambda_m \delta_n},$$

$$f_5 = \frac{(I_{17} I_{12} + I_{11} I_{27})}{\left(I_{12}^2 - I_{11} I_{21}\right)}, f_6 = \frac{(I_{18} I_{12} + I_{11} I_{28})}{\left(I_{12}^2 - I_{11} I_{21}\right)}, f_7 = \frac{(I_{19} I_{12} + I_{11} I_{29})}{\left(I_{12}^2 - I_{11} I_{21}\right)}.$$

Appendix F

$$l_{11}^1 = (l_{11} + l_{16} h_{11} + l_{17} h_{21}), l_{12}^1 = (l_{12} + l_{16} h_{12} + l_{17} h_{22}), l_{13}^1 = (l_{13} + l_{16} h_{13} + l_{17} h_{23}),$$
$$l_{21}^1 = (l_{21} + l_{24} h_{11} + l_{25} h_{21}), l_{22}^1 = (l_{22} + l_{24} h_{12} + l_{25} h_{22}), l_{23}^1 = (l_{23} + l_{24} h_{13} + l_{25} h_{23}),$$

$$l_{31}^1 = (l_{31} + l_{34} h_{11} + l_{35} h_{21}), l_{32}^1 = (l_{32} + l_{34} h_{12} + l_{35} h_{22}), l_{33}^1 = (l_{33} + l_{34} h_{13} + l_{35} h_{23}),$$
$$h_{11} = \frac{(l_{45} l_{51} - l_{41} l_{55})}{(l_{44} l_{55} - l_{45} l_{54})}, h_{12} = \frac{(l_{45} l_{52} - l_{42} l_{55})}{(l_{44} l_{55} - l_{45} l_{54})}, h_{13} = \frac{(l_{45} l_{53} - l_{43} l_{55})}{(l_{44} l_{55} - l_{45} l_{54})},$$
$$h_{21} = \frac{(l_{41} l_{54} - l_{44} l_{51})}{(l_{44} l_{55} - l_{45} l_{54})}, h_{22} = \frac{(l_{42} l_{54} - l_{44} l_{52})}{(l_{44} l_{55} - l_{45} l_{54})}, h_{23} = \frac{(l_{43} l_{54} - l_{44} l_{53})}{(l_{44} l_{55} - l_{45} l_{54})}.$$

Appendix G

$$\overline{j_0} = j_0 - \left(l_{12}^1 a_{14} + l_{13}^1 a_{24}\right),\ j_0^* = \left(l_{14}^1 a_{14} + l_{15}^1 a_{24}\right),$$
$$b_{11} = \left(l_{11}^1 + l_{12}^1 a_{11} + l_{13}^1 a_{21}\right),\ b_{12} = \left(n_1^1 + l_{12}^1 a_{12} + l_{13}^1 a_{22}\right),$$
$$b_{13} = \left(n_2^1 + l_{14}^1 a_{11} + l_{15}^1 a_{21}\right),\ b_{14} = \left(n_3 + l_{12}^1 a_{13} + l_{13}^1 a_{23}\right),$$
$$b_{15} = \left(l_{14}^1 a_{12} + l_{15}^1 a_{22}\right),\ b_{16} = \left(n_4^1 + l_{14}^1 a_{13} + l_{15}^1 a_{23}\right),$$

$$a_{11} = -\frac{\left(l_{21}^1 l_{33}^1 - l_{23} l_{31}\right)}{\left(l_{22}^1 l_{33}^1 - l_{23}^1 l_{32}^1\right)},\ a_{12} = -\frac{\left(n_6 l_{33}^1 - n_8 l_{23}^1\right)}{\left(l_{22}^1 l_{33}^1 - l_{23}^1 l_{32}^1\right)},$$
$$\frac{a_{13} = -\frac{\left(n_7 l_{33}^1 - n_9 l_{23}^1\right)}{\left(l_{22}^1 l_{33}^1 - l_{23}^1 l_{32}^1\right)},\ a_{14} = \left(-\lambda_m \overline{\overline{j_5}} l_{33}^1 + \delta_n \overline{\overline{j_5^*}} l_{23}^1\right)}{\left(l_{22}^1 l_{33}^1 - l_{23}^1 l_{32}^1\right)}.$$

References

[1] Gholipour G, Zhang C, Mousavi AA. Nonlinear failure analysis of bridge pier subjected to vessel impact combined with blast loads. Ocean Eng 2021;234:109209. https://doi.org/10.1016/j.oceaneng.2021.109209.

[2] Maazoun A, Matthys S, Belkassem B, Atoui O, Lecompte D. Experimental study of the bond interaction between CFRP and concrete under blast loading. Compos Struct 2021;277:114608. https://doi.org/10.1016/j.compstruct.2021.114608.

[3] Roy T, Matsagar V. Probabilistic framework for failure investigation of reinforced concrete wall panel under dynamic blast loads. Eng Fail Anal 2021;125:105368. https://doi.org/10.1016/j.engfailanal.2021.105368.

[4] Lam N, Mendis P, Ngo T. Response spectrum solutions for blast loading. electron. J Struct Eng 2004;4:28–44.

[5] Karmakar S, Shaw A. Response of R.C. plates under blast loading using FEM-SPH coupled method. Eng Fail Anal 2021;125:105409. https://doi.org/10.1016/j.engfailanal.2021.105409.

[6] Gao C, Kong X, Fang Q, Hong J, Wang Y. Numerical investigation on free air blast loads generated from center-initiated cylindrical charges with varied aspect ratio in arbitrary orientation. Def Technol 2021; In Press, Corrected Proof. 10.1016/j.dt.2021.07.013.

[7] Le VT, Ghazlan A, Nguyen T, Ngo T. Performance of bio-inspired cross-laminated timber under blast loading – A numerical study. Compos Struct 2021;260:113524. https://doi.org/10.1016/j.compstruct.2020.113524.

[8] Xiao W, Andrae M, Steyerer M, Gebbeken N. Investigations of blast loads on a two-storeyed building with a gable roof: Full-scale experiments and numerical study. J Build Eng 2021;43:103111. https://doi.org/10.1016/j.jobe.2021.103111.

[9] Usta F, Türkmen HS, Scarpa F. Low-velocity impact resistance of composite sandwich panels with various types of auxetic and non-auxetic core structures. Thin-Walled Struct 2021;163:107738. https://doi.org/10.1016/j.tws.2021.107738.

[10] Dong K, Panahi-Sarmad M, Cui Z, Huang X, Xiao X. Electro-induced shape memory effect of 4D printed auxetic composite using PLA/TPU/CNT filament embedded synergistically with continuous carbon fiber: A theoretical & experimental analysis. Compos Part B Eng 2021;220:108994. https://doi.org/10.1016/j.compositesb.2021.108994.

[11] Dutta S, Menon HG, Hariprasad MP, Krishnan A, Shankar B. Study of auxetic beams under bending: A finite element approach. Mater Today Proc 2020; In Press, Corrected Proof. 10.1016/j.matpr.2020.10.479.

[12] Li C, Shen H-S, Wang H, Yu Z. Large amplitude vibration of sandwich plates with functionally graded auxetic 3D lattice core. Int J Mech Sci 2020;174:105472. https://doi.org/10.1016/j.ijmecsci.2020.105472.

[13] Li C, Shen H-S, Wang H. Nonlinear dynamic response of sandwich plates with functionally graded auxetic 3D lattice core. Nonlinear Dyn 2020;100(4):3235–52. https://doi.org/10.1007/s11071-020-05686-4.

[14] Gao J, Wang L, Xiao Mi, Gao L, Li P. An isogeometric approach to topological optimization design of auxetic composites with tri-material micro-architectures. Compos Struct 2021;271:114163. https://doi.org/10.1016/j.compstruct.2021.114163.

[15] Van Quyen N, Van Thanh N, Quan TQ, Duc ND. Nonlinear forced vibration of sandwich cylindrical panel with negative Poisson's ratio auxetic honeycombs core and CNTRC face sheets. Thin-Walled Struct 2021;162:107571. https://doi.org/10.1016/j.tws.2021.107571.

[16] Li C, Shen HS, Yang J, Wang H. Low-velocity impact response of sandwich plates with GRC face sheets and FG auxetic 3D lattice cores. Eng Anal Bound Elem 2021;132:335–44. https://doi.org/10.1016/j.enganabound.2021.08.002.

[17] Yang J, Huang X-H, Shen H-S. Nonlinear vibration of temperature-dependent FG-CNTRC laminated plates with negative Poisson's ratio. Thin Wall Struct 2020;148:106514. https://doi.org/10.1016/j.tws.2019.106514.

[18] Cong PH, Duc ND. Nonlinear dynamic analysis of porous eccentrically stiffened double curved shallow auxetic shells in thermal environments. Thin-Walled Struct 2021;163:107748. https://doi.org/10.1016/j.tws.2021.107748.

[19] Tran TT, Pham QH, Nguyen-Thoi T, Van TT. Dynamic analysis of sandwich auxetic honeycomb plates subjected to moving oscillator load on elastic foundation. Adv Mater Sci Eng 2020;2020:1–16. https://doi.org/10.1155/2020/6309130.
[20] Yu Y, Shen H-S. A comparison of nonlinear vibration and bending of hybrid CNTRC/metal laminated plates with positive and negative Poisson's ratios. Int J Mech Sci 2020;183:105790. https://doi.org/10.1016/j.ijmecsci.2020.105790.
[21] Gohar S, Hussain G, Ilyas M, Ali A. Performance of 3D printed topologically optimized novel auxetic structures under compressive loading: experimental and FE analyses. J Mater Res Technol 2021;15:394–408. https://doi.org/10.1016/j.jmrt.2021.07.149.
[22] Gao Q, Liao W-H. Energy absorption of thin walled tube filled with gradient auxetic structures-theory and simulation. Int J Mech Sci 2021;201:106475. https://doi.org/10.1016/j.ijmecsci.2021.106475.
[23] Żur KK, Arefi M, Kim J, Reddy JN. Free vibration and buckling analyses of magneto-electro-elastic FGM nanoplates based on nonlocal modified higher-order sinusoidal shear deformation theory. Compos Part B Eng 2020;182:107601. https://doi.org/10.1016/j.compositesb:2019.107601.
[24] Arefi M, Amabili M. A comprehensive electro-magneto-elastic buckling and bending analyses of three-layered doubly curved nanoshell, based on nonlocal three-dimensional theory. Compos Struct 2021;257:113100. https://doi.org/10.1016/j.compstruct.2020.113100.
[25] Vinyas M, Sunny KK, Harursampath D, Nguyen-Thoi T, Loja MAR. Influence of interphase on the multi-physics coupled frequency of three-phase smart magneto-electro-elastic composite plates. Compos Struct 2019;226:111254. https://doi.org/10.1016/j.compstruct.2019.111254.
[26] Zhu S, Sun J, Tong Z, Li Q, Zhou Z, Xu X. Post-buckling analysis of magneto-electro-elastic composite cylindrical shells subjected to multi-field coupled loadings. Compos Struct 2021;270:114061. https://doi.org/10.1016/j.compstruct.2021.114061.
[27] Dat ND, Quan TQ, Mahesh V, Duc ND. Analytical solutions for nonlinear magneto-electro-elastic vibration of smart sandwich plate with carbon nanotube reinforced nanocomposite core in hygrothermal environment. Int J Mech Sci 2020;186:105906. https://doi.org/10.1016/j.ijmecsci.2020.105906.
[28] Zhou L, Tang J, Tian W, Xue B, Li X. A multi-physics coupling cell-based smoothed finite element micromechanical model for the transient response of magneto-electro-elastic structures with the asymptotic homogenization method. Thin-Walled Struct 2021;165:107991. https://doi.org/10.1016/j.tws.2021.107991.
[29] Ye W, Liu J, Fang H, Lin G. Numerical solutions for magneto–electro–elastic laminated plates resting on Winkler foundation or elastic half-space. Comput Math with Appl 2020;79(8):2388–410. https://doi.org/10.1016/j.camwa.2019.11.007.
[30] Shojaeefard MH, Mahinzare M, Safarpour H, Saeidi Googarchin H, Ghadiri M. Free vibration of an ultra-fast-rotating-induced cylindrical nano-shell resting on a Winkler foundation under thermo-electro-magneto-elastic condition. Appl Math Model 2018;61:255–79. https://doi.org/10.1016/j.apm.2018.04.015.
[31] Chen J, Chen H, Pan E, Heyliger PR. Modal analysis of magneto-electro-elastic plates using the state-vector approach. J Sound Vib 2007;304(3-5):722–34. https://doi.org/10.1016/j.jsv.2007.03.021.
[32] Xu X-J, Meng J-M. A size-dependent elastic theory for magneto-electro-elastic materials. Eur J Mech A/Solids 2021;86:104198. https://doi.org/10.1016/j.euromechsol.2020.104198.
[33] Singh PN, Sundararajan V, Das YC. Large amplitude vibration of some moderately thick structural elements. J Sound Vib 1974;36(3):375–87. https://doi.org/10.1016/S0022-460X(74)80217-8.
[34] Chen L-W, Doong J-L. Large amplitude vibration of an initially stressed moderately thick plate. J Sound Vib 1983;89(4):499–508. https://doi.org/10.1016/0022-460X(83)90351-6.
[35] Bhimaraddi A. Large amplitude vibrations of imperfect antisymmetric angle-ply laminated plates. J Sound Vib 1993;162:457–70. https://doi.org/10.1006/jsvi.1993.1133.
[36] Wang ZX, Shen HS. Nonlinear vibration and bending of sandwich plates with nanotube-reinforced composite face sheets. Compos Part B Eng 2012;43(2):411–21. https://doi.org/10.1016/j.compositesb.2011.04.040.
[37] Brush DD, Almroth BO. Buckling of bars, plates and shells. Mc. Graw-Hill 1975.
[38] Reddy JN. Mechanics of laminated composite plates and shells: Theory and analysis. Boca Raton: CRC Press; 2004.